
Journal of Electronic & Information Systems

Volume 1 | Issue 1 | 2019 April | ISSN 2661-3204 (Online)

01



**BILINGUAL
PUBLISHING CO.**
Pioneer of Global Academics Since 1984

Editor-in-Chief

Dr. Chin-Ling Chen

Chaoyang University of Technology, Taiwan

Editorial Board Members

Chong Huang, United States	Husam Abduldaem Mohammed, Iraq
Yoshifumi Manabe, Japan	Muhammet Nuri Seyman, Turkey
Hao Xu, United States	Neelamadhab Padhy, India
Shicheng Guo, United States	Ali Mohsen Zadeh, Iran
Leila Ghabeli, Iran	Oye Nathaniel David, Nigeria
Diego Real Mañez, Spain	Xiru Wu, China
Senthil Kumar Kumaraswamy, India	Yashar Hashemi, Iran
Santhan Kumar Cherukuri, India	Ali Ranjbaran, Iran
Asit Kumar Gain, Australia	Abdul Qayyum, France
Jue-Sam Chou, Taiwan	JianChao Luo, China
Sedigheh Ghofrani, Iran	Alberto Huertas Celdran, Ireland
Yu Tao, China	Maxim A. Dulebenets, United States
Lianggui Liu, China	Yanxiang Zhang, China
Vandana Roy, India	Alex Michailovich Asavin, Russian Federation
Mehmet Ali Akinlar, Turkey	Jafar Ramadhan Mohammed, Iraq
Jun Zhu, China	Shitharth Selvarajan, India
Zulkifli Bin Mohd Rosli, Malaysia	Schekeb Fateh, Switzerland
Radu Emanuil Petruse, Romania	Alexandre Jean Rene Serres, Brazil
Saima Saddiq, Pakistan	Dadmehr Rahbari, Iran
Saleh Mobayen, Iran	Junxuan Zhao, United States
Asaf Tolga Ulgen, Turkey	Jun Shen, China
Xue-Jun Xie, China	Xinggang Yan, United Kingdom
Mehmet Hacibeyoglu, Turkey	Yuan Tian, China
Prince Winston D, India	Abdollah Doosti-Aref, Iran
Ping Ding, China	Mingxiong Zhao, China
Youqiao Ma, Canada	Hamed Abdollahzadeh, Iran
Marlon Mauricio Hernandez Cely, Brazil	Falu Weng, China
Amirali Abbasi, Iran	Waleed Saad Hilmy, Egypt
Ge Song, United States	Qilei Li, China
Rui Min, China	Quang Ngoc Nguyen, Japan
P. D. Sahare, India	Fei Wang, China
Volodymyr Gennadievich Skobelev, Ukraine	Xiaofeng Yuan, China
Hui Chen, China	Vahdat Nazerian, Iran
M.M. Kamruzzaman, Bangladesh	Yanling Wei, Belgium
Seyed Saeid Moosavi Anchehpoli, Iran	Kamarulzaman Kamarudin, Malaysia
Sayed Alireza Sadrossadat, Iran	Tajudeen Olawale Olasupo, United States
Fa Wang, United States	Md. Mahbubur Rahman, Korea
Tingting Zhao, China	Igor Simplicio Mokem Fokou, Cameroon
Sasmita Mohapatra, India	Héctor F. Migallón, Spain
Akram Sheikhi, Iran	Ning Cai, China

Volume 1 Issue 1 • April 2019 • ISSN 2661-3204 (Online)

Journal of Electronic & Information Systems

Editor-in-Chief
Dr. Chin-Ling Chen



**BILINGUAL
PUBLISHING CO.**
Pioneer of Global Academics Since 1984

Contents

Editorial

1 A Foreword from the Editor-in-Chief

Chin-Ling Chen

Article

3 Measurement for Phase Difference Rate without Phase Ambiguity

Yu Tao

18 A Novel Image Encryption Scheme Based on Reversible Cellular Automata

Zeinab Mehrnahad AliMohammad Latif

26 Computation Offloading and Scheduling in Edge-Fog Cloud Computing

Dadmehr Rahbari Mohsen Nickray

37 Development of IoT Based Mobile Robot for Automated Guided Vehicle Application

M. A. S. M. Alhaddad K. Kamarudin

Copyright

Journal of Electronic & Information Systems is licensed under a Creative Commons-Non-Commercial 4.0 International Copyright (CC BY- NC4.0). Readers shall have the right to copy and distribute articles in this journal in any form in any medium, and may also modify, convert or create on the basis of articles. In sharing and using articles in this journal, the user must indicate the author and source, and mark the changes made in articles. Copyright © BILINGUAL PUBLISHING CO. All Rights Reserved.



EDITORIAL

A Foreword from the Editor-in-Chief

Chin-Ling Chen*

Chaoyang University of Technology, Taiwan

ARTICLE INFO

Article history

Received: 25 October 2019

Accepted: 28 October 2019

Published Online: 31 October 2019

Due to the advancement of information technology, Journal of Electronic & Information Systems aims to discover innovative methods, theories and studies in its field by publishing original articles, case studies and comprehensive reviews. Journal of Electronic & Information Systems provides a wide range of readers and authors. A good communication platform, in the expectation, the first issue of the first volume was first published.

Journal of Electronic & Information Systems publishes original research papers that it has officially applied for the electronic ISSN (Online) to be 2661-3204. The current Vol. 1 No. 1 will be issued with electronic publications. In this issue of the public collection section, there are included four articles:

The First article: Measurement for phase difference rate without phase ambiguity. The purpose of the paper is the direction finding solution at the midpoint of a single base array is given for and the several functions relation between phase and frequency is also described. Then, the expression of phase difference rate is described based on the multichannel phase difference measurement. Thus, the function expression can be obtained that is equivalence with the quondam differential function of path differ-

ence and that is nothing to do with the difference item of wavelength integer. On this basic, several parameters are analyzed by using the method of phase difference measurement without phase ambiguity. The research results in this paper are related to engineering practical design related to the phase measuring.

The Second article: A Novel Image Encryption Scheme Based on Reversible Cellular Automata. In this paper, a new scheme for image encryption is presented by reversible cellular automata. Due to reversibility of used cellular automata, decryption scheme can reversely be applied. The experimental results show that encrypted image is suitable visually and this scheme has satisfied quantitative performance.

The Third Article: Computation Offloading and Scheduling in Edge-Fog Cloud Computing. Nowadays, resource allocation and task scheduling in the cloud environment face many challenges. In this article, we review the resource allocation and task scheduling methods in Cloud, Edge and Fog environments, such as traditional, heuristic, and meta-heuristics. The authors also categorize the researches related to task offloading in Mobile Cloud Computing (MCC), Mobile Edge Computing (MEC), and

*Corresponding Author:

Chin-Ling Chen,
Chaoyang University of Technology; Taiwan;
Email: clc@cyut.edu.tw

Mobile Fog Computing (MFC). Our categorization criteria include the issue, proposed strategy, objectives, framework, and test environment.

The Fourth Article: Development of IoT Based Mobile Robot for Automated Guided Vehicle Application.

Mobile robot has been one of the researches focuses in this era due to the demands in automation. The advances in the navigation technology allows the AGV to be used for many tasks. This paper will therefore discuss the development of Internet of Things (IoT) bases mobile robot for AGV application. In this project a mobile robot platform is designed and fabricated. The results show that the prototype is able to follow line and go to any location that was preregistered from the App through the IoT. The mobile robot is also able to avoid collision and any obstacles that exist on its way to perform any task inside the workplace.

In addition, Journal of Electronic & Information Systems publishes original research papers that offers pro-

fessional review and publication to freely disseminate research findings in areas of Networks and Telecommunication, Human–Computer Interaction, Data Management, High Voltage Engineering and more. The Journal focuses on innovations of research methods at all stages and is committed to provide theoretical and practical experience for all those who are involved in these fields.

Journal of Electronic & Information Systems aims to discover innovative methods, theories and studies in its field by publishing original articles, case studies and comprehensive reviews.

This journal will continue to move towards the internationalization of journals. Thanks to all readers for their long-term support, and welcome you to provide the latest research results to the journal for sharing and exchange.

Journal of Electronic & Information Systems
Chin-Ling Chen



ARTICLE

Measurement for Phase Difference Rate without Phase Ambiguity

Yu Tao*

51 st Research Institute of CETC, Shanghai, 201802, China

ARTICLE INFO

Article history

Received: 1 March 2019

Accepted: 9 September 2019

Published Online: 18 October 2019

Keywords:

Phase difference rate

Phase ambiguity

Doppler frequency shift

Path difference

Passive location

ABSTRACT

Firstly, the direction finding solution at the midpoint of a single base array is given for the purpose of this paper and the several functions relation between phase and frequency is also described. Then, the expression of phase difference rate is described based on the multichannel phase difference measurement. With stripping time difference item correspond to the baseline length from phase difference rate, a function is extracted which signifies the differential characteristics of wavelength integer and phase difference in a unit of length. Simulation calculation found that the variation of differential function of path difference in a unit of length is very regular. The corresponding corrected value can be determined directly by distinguishing the range of differential item of phase difference obtained by actual measurement. Thus, the function expression can be obtained that is equivalent with the quondam differential function of path difference and that is nothing to do with the difference item of wavelength integer. On this basis, several parameters are analyzed by using the method of phase difference measurement without phase ambiguity. The research results in this paper may provide a powerful technical support for engineering practical design related to the phase measuring.

1. Introduction

The phase difference rate can be used for passive localization^[1-5]. There are two main methods to obtain the phase difference rate^[6]. One is to extract the phase difference rate by measuring phase difference sequences and using algorithms such as difference, Kalman filtering and linear fitting^[7]. The other is to calculate the phase difference rate by indirectly measuring the output frequency difference between two comparison channels based on phase discrimination^[8-10]. The previous method must be measured in a row to get enough phase difference sequences, and it needs to increase the measurement accuracy by extending the observation time. It's possible that the obtained phase difference is not linear. In

the case of the short baseline application, the equivalent measurement time is very short because the frequency difference interval that can be measured is too small, so that the posterior method can make the measurement error become very large. Therefrom, the prediction accuracy of the phase difference rate is hard to improve.

In the existing passive positioning analysis based on the phase difference measurement, the integer value of the wavelength is looked at as a constant value. And it's thought that the phase difference rate will have nothing to do with the integer of wavelengths after the differential treatment. That is, the difference of phase difference is not ambiguous^[11-14]. But the analysis shows whether the phase difference rate is derived based on the relationship

*Corresponding Author:

Yu Tao,

51 st Research Institute of CETC, Shanghai, 201802, China;

Email: tyt0803@163.com

between phase and frequency or is obtained by making differential treatment directly to phase difference measurement based on the time series, it is related not only to the difference item of phase difference, but also to the difference item of the difference value of the integer of wavelengths. Moreover, there is mutual jump phenomenon between the difference item of phase difference and the difference item of the difference value of the integer of wavelengths.

Based on the functional relationship between phase shift and Doppler frequency shift^[15], the authors have proved mathematically that the phase difference rate can be obtained in real time by using the short baseline linear array and the multichannel phase shift detection^[16]. On the basis of this study, the author further studies the method to detect the phase difference rate without phase ambiguity.

Firstly, the expression of the phase difference rate by using the phase-frequency function is derived based on multichannel phase difference measurement. Then the time difference term corresponding to the baseline length is separated from the phase difference rate. The resulting is to obtain a function that can represent the difference characteristic of difference value in unit length. The subsequent simulation results show that the variation of the difference function on the unit length is very regular. The corresponding correction number can be determined directly by distinguishing the range of difference of phase difference, that the range is obtained by the actual measurement. A function expression can be obtained independent of the difference term of the integer of wavelengths as well as equivalent to the difference function of path difference in unit length.

The author's research results show that, based on the multichannel phase difference measurement, the phase difference rate can be directly obtained only by using the measured value of phase difference, and by using the jump rule of difference including the difference value of the integer of wavelengths as well as the phase difference under the condition that the difference value of integer of wavelengths is unknown. The results of this study lay a very important foundation for the engineering application of phase difference location.

Based on the function relation between the phase shift and the frequency shift, the analysis showed that many parameters in passive location is related to the testing of phase difference rate. Many kinematic positioning parameters can be converted into the function associated with the phase difference rate. Therefore, once the detection to the phase difference rate can be realized without phase ambiguity, these parameters directly related to the phase

difference rate can be all solved without ambiguity. Furthermore, the physical meaning of some parameters can be understood more deeply by means of the difference expression of path difference.

2. A Simplified Solution for the Direction Finding at the Midpoint of a Single Base Array

2.1 Introduction

As the basis of the follow-up chapter, in this chapter, a single base direction finding equation which is only related to the path difference measurement is obtained by simplifying the one-dimensional path difference equation based on double-base array. Although the three-station direction finding method with two baselines obtained by using the path difference measurement and geometrical assistant relation is suitable for arbitrary baseline length, it is most desirable to realize the direction finding of double stations from the perspective of engineering application.

2.2 One Dimensional Double-base Direction Finding Solution

For the one-dimensional double-base phase interference array shown in Figure 1, the path difference between the adjacent two baselines is:

$$\Delta r_i = r_i - r_{i+1} \quad (1)$$

$$\Delta r_{i+1} = r_{i+1} - r_{i+2} \quad (2)$$

If the center point of the whole array is used as the origin of coordinates, then the following two geometric auxiliary equations can be listed by the cosine theorem:

$$r_i^2 = r_{i+1}^2 + d_i^2 - 2d_i r_{i+1} \cos(90 + \theta_{i+1}) = r_{i+1}^2 + d_i^2 + 2d_i r_{i+1} \sin \theta_{i+1} \quad (3)$$

$$r_{i+2}^2 = r_{i+1}^2 + d_{i+1}^2 - 2d_{i+1} r_{i+1} \cos(90 - \theta_{i+1}) = r_{i+1}^2 + d_{i+1}^2 - 2d_{i+1} r_{i+1} \sin \theta_{i+1} \quad (4)$$

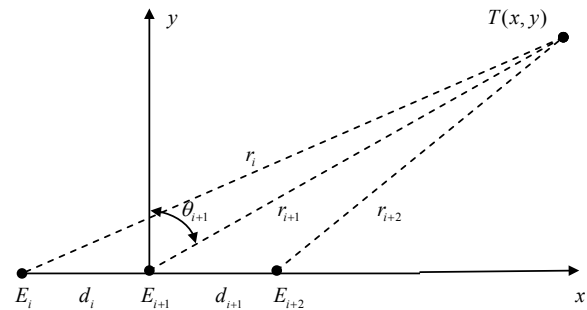


Figure 1. One-dimensional double-base array

Due to: $x = r_{i+1} \sin \theta_{i+1}$, Therefore, the geometric auxiliary equation can be rewritten as:

$$r_i^2 = r_{i+1}^2 + d_i^2 + 2d_i x \quad (5)$$

$$r_{i+2}^2 = r_{i+1}^2 + d_{i+1}^2 - 2d_{i+1} x \quad (6)$$

Where: d_i is the length of single baseline; x is the x-coordinate of rectangular coordinate system.

At this point, if the path difference (1) and (2) between two adjacent baselines are substituted into the geometric auxiliary equations (5) and (6), then the following binary primary linear equations can be obtained after rearrangement:

$$2d_i x - 2\Delta r_i r_i = -d_i^2 + \Delta r_i^2 \quad (7)$$

$$2d_{i+1} x - 2\Delta r_{i+1} r_{i+1} = d_{i+1}^2 - \Delta r_{i+1}^2 \quad (8)$$

From this, the horizontal distance of the target can be directly solved out:

$$x = \frac{(d_i^2 - \Delta r_i^2)\Delta r_{i+1} + (d_{i+1}^2 - \Delta r_{i+1}^2)\Delta r_i}{2(\Delta r_i d_{i+1} - \Delta r_{i+1} d_i)} \quad (9)$$

And the radial distance of the target:

$$r_{i+1} = \frac{(d_i^2 - \Delta r_i^2)d_{i+1} + (d_{i+1}^2 - \Delta r_{i+1}^2)d_i}{2(\Delta r_i d_{i+1} - \Delta r_{i+1} d_i)} \quad (10)$$

From this, the arrival angle of the target can be obtained:

$$\sin \theta_{i+1} = \frac{x}{r_{i+1}} = \frac{(d_i^2 - \Delta r_i^2)\Delta r_{i+1} + (d_{i+1}^2 - \Delta r_{i+1}^2)\Delta r_i}{(d_i^2 - \Delta r_i^2)d_{i+1} + (d_{i+1}^2 - \Delta r_{i+1}^2)d_i} \quad (11)$$

2.3 Approximate Simplified Solution

For one-dimensional double-base direction finding equation:

$$\sin \theta = \frac{(d^2 - \Delta r_1^2)\Delta r_2 + (d^2 - \Delta r_2^2)\Delta r_1}{d(2d^2 - \Delta r_1^2 - \Delta r_2^2)} \quad (12)$$

If the approximate treatment is done for the higher-order terms of path difference: $\Delta r_1 \approx \Delta r_2$, accordingly, after simplification, there is:

$$\sin \theta \approx \frac{(d^2 - \Delta r_2^2)(\Delta r_1 + \Delta r_2)}{2d(d^2 - \Delta r_1^2)} = \frac{(\Delta r_1 + \Delta r_2)}{2d} \quad (13)$$

For:

$$\Delta r_{13} = r_1 - r_3 = (r_1 - r_2) + (r_2 - r_3) = \Delta r_1 + \Delta r_2 \quad (14)$$

From this, the single base direction finding solution only related to the measurement of path difference is obtained:

$$\sin \theta = \frac{\Delta r_{13}}{2d} \quad (15)$$

Note that the reference point for a single base direction finding is at the mid-point of a single baseline, not at the left or right end of a single baseline.

The simulation results show that the single base direction-finding formula (15) obtained from the approximation simplification is correct not only for short baselines, but also for longer baselines.

2.4 Summary

One of the important applications of single-base direction finding is the direction-finding using time difference measurement based on long baseline. As a high-precision direction finding method for passive detection of military applications, the research on time difference detection technology has made a significant breakthrough in the past 40 years, but the relevant research so far mainly focuses on the short baseline time difference measurement method^[17-20]. On the one hand it's a tactical need, on the other hand it involves the mathematical models. The existing direction finding formula based on short baseline is only a very approximate calculation method. If it is extended to long baseline measurement, the calculation accuracy will become worse and cannot be applied. It seems that the results can be given in form by using the existing approximate short baseline direction-finding formula, but the mathematical description is incomplete, and more importantly, it is difficult to accurately analyze the problems related to the long baseline.

Obviously, based on the principle that the direction finding precision is proportional to the length of the baseline, if the model suitable for the time difference measurement of the long baseline can be given mathematically, the direction finding performance of the ultra-precision should be obtained.

3. Some Function Relations between the Phase and Frequency

3.1 Phase Difference Positioning Equation

If the phase-interferometer is used for passive detection

of the target, and the phase-interferometer is assumed to only use the single-base antenna array as shown in Figure 2, the distance formula based on the phase shift measurement is as follows:

$$r_i = \lambda \left(n_i + \frac{\phi_i}{2\pi} \right) \quad (16)$$

Where: r_i is the radial distance; λ the wavelength; n_i the number of wavelengths; ϕ_i the phase shift measured by the Phase detector unit.

According to the relation (16) between phase shift and distance, the path difference Δr_i between two radial distance corresponding to the array elements E_i and E_{i+1} of a single baseline can be determined by the phase difference measurement, and the phase difference localization equation can be obtained whose form is completely similar to the time difference localization equation:

$$\Delta r_i = r_i - r_{i+1} = \lambda \left(n_i - n_{i+1} + \frac{\phi_i - \phi_{i+1}}{2\pi} \right) = \lambda \left(\Delta n_i + \frac{\Delta \phi_i}{2\pi} \right) \quad (17)$$

Where: $\Delta n_i = n_i - n_{i+1}$ is the difference value of wavelength number contained in the path difference; $\Delta \phi_i = \phi_i - \phi_{i+1}$ the phase difference between two elements.

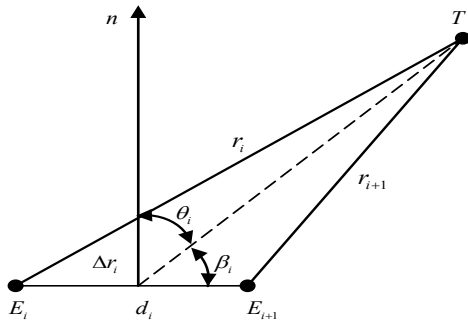


Figure 2. Schematic diagram of single base array

3.2 Direction Finding Solution Using Single Baseline based on Phase Difference Measurement

Based on phase difference positioning equation, the direction finding solution based on phase difference measurement can be directly obtained by further using the expression form of single base middle point direction finding instead of the existing short baseline phase interference direction finding concept:

$$\sin \theta_i = \frac{\Delta r_i}{d_i} = \frac{\lambda}{d_i} \left(\Delta n_i + \frac{\Delta \phi_i}{2\pi} \right) \quad (18)$$

The direction-finding formula given here can be applied to longer baselines from a purely mathematical definition,

but note that the reference point of the measurement is at the midpoint of the baseline.

3.3 The Function Relation between Phase Difference and Frequency Shift

A Doppler receiver is installed on the airborne platform to detect stationary or slow-moving targets on the ground, and the Doppler frequency shift received at the middle point of a single base is:

$$\lambda f_{di} = v \cos \beta_i \quad (19)$$

Where: f_{di} is Doppler frequency shift; v the speed of the airplane; β_i the leading angle.

According to the reciprocal relationship between the arrival angle and the leading angle: $\sin \theta_i = \cos \beta_i$, using the direction finding formula (19) of the single base midpoint based on the phase difference measurement, the leading angle can be expressed as:

$$\cos \beta_i = \frac{\Delta r_i}{d_i} = \frac{\lambda}{d_i} \left(\Delta n_i + \frac{\Delta \phi_i}{2\pi} \right) \quad (20)$$

And once expression (20) is substituted into the Doppler shift expression (19), the functional relationship between phase difference and Doppler shift is obtained:

$$f_{di} = \frac{v}{d_i} \left(\Delta n_i + \frac{\Delta \phi_i}{2\pi} \right) \quad (21)$$

3.4 The Function Relation between the Change Rate of Phase Shift and Frequency Shift

If the differentiating with respect to time is applied to both sides of the phase-distance expression (16), then there is:

$$\frac{\partial r_i}{\partial t} = \frac{\lambda}{2\pi} \frac{\partial \phi_i}{\partial t} \quad (22)$$

According to the relation between the change rate of radial distance and Doppler frequency shift:

$$\frac{\partial r_i}{\partial t} = v_{ri} = \lambda f_{di} \quad (23)$$

It can be proved that:

$$\frac{\partial \phi_i}{\partial t} = 2\pi f_{di} \quad (24)$$

3.5 The relation between the phase difference rate and frequency difference

If the differential with respect to time is applied to both

sides of the relation (17) of phase difference - distance difference, then:

$$\frac{\partial \Delta r_i}{\partial t} = \frac{\lambda}{2\pi} \frac{\partial \Delta \phi}{\partial t} \quad (25)$$

According to the relation between the change rate of radial distance and Doppler frequency shift:

$$\frac{\partial r_i}{\partial t} = v_{ri} = \lambda f_{di} \quad (26)$$

Based on the same process, the relation between the phase difference rate and frequency difference can be obtained:

$$\frac{\partial \Delta \phi}{\partial t} = 2\pi \Delta f_d \quad (27)$$

Where: $\Delta f_d = f_{d1} - f_{d2}$.

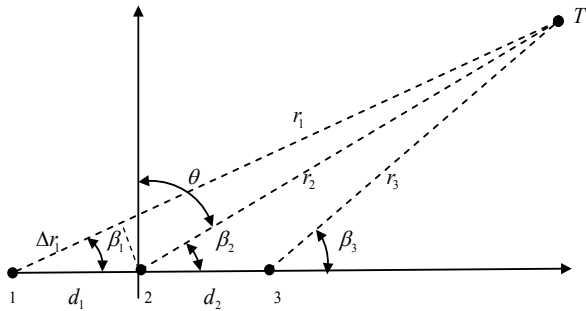


Figure 3. The one-dimensional double base array with three units

It is proved that the phase difference rate can be obtained by detecting the Doppler frequency difference. According to the relationship Eq.(24) between Doppler shift and the change rate of phase shift, the Doppler shift value corresponding to a certain radial distance actually needs to be obtained by difference of two phase values. Therefore, in order to obtain the Doppler frequency difference, three phase shifts need to be detected simultaneously, that is, the one-dimensional double base array with three units as shown in Figure 3 needs to be adopted from the implementation method of measurement.

4. Phase Difference Rate Based on Multichannel Phase Difference Measurement

4.1 The Change Rate of Phase Shift Obtained by Detecting Phase Difference

The change rate of radial distance is the radial velocity of

the target:

$$\frac{\partial r_i}{\partial t} = v_{ri} = v \sin \theta \quad (28)$$

Where: v is the flight speed of the aerial carrier, and v_{ri} the radial speed.

Use the relationship between the change rate of distance and the change rate of phase shift Eq.(22) :

$$\frac{\partial r_i}{\partial t} = \frac{\lambda}{2\pi} \frac{\partial \phi_i}{\partial t} \quad (29)$$

And use the direction finding formula Eq.(18) of single-base midpoint based on phase difference measurement:

$$\sin \theta \approx \frac{\Delta r_i}{d} = \frac{\lambda}{d} \left(\Delta n_i + \frac{\Delta \phi_i}{2\pi} \right) \quad (30)$$

It can be proved that the formula of the change rate of phase shift based on the phase difference measurement is:

$$\frac{\partial \phi_i}{\partial t} = \frac{2\pi v}{d} \left(\Delta n_i + \frac{\Delta \phi_i}{2\pi} \right) \quad (31)$$

4.2 The Phase Difference Rate Obtained by Detecting the Phase Difference

Directly from formula Eq.(31), there are:

$$\begin{aligned} \frac{\partial \Delta \phi}{\partial t} &= \frac{\partial \phi_1}{\partial t} - \frac{\partial \phi_2}{\partial t} \\ &= \frac{2\pi v}{d_i} \left(\Delta n_i + \frac{\Delta \phi_i}{2\pi} \right) - \frac{2\pi v}{d_{(i+1)}} \left(\Delta n_{(i+1)} + \frac{\Delta \phi_{(i+1)}}{2\pi} \right) \\ &= 2\pi v \left[\left(\frac{\Delta n_i}{d_i} - \frac{\Delta n_{(i+1)}}{d_{(i+1)}} \right) + \left(\frac{\Delta \phi_i}{2\pi d_i} - \frac{\Delta \phi_{(i+1)}}{2\pi d_{(i+1)}} \right) \right] \end{aligned} \quad (32)$$

For the double-base linear array that is equidistant, that is, when $d = d_1 = d_2$, there is:

$$\frac{\partial \Delta \phi}{\partial t} = \frac{2\pi v}{d} \left[(\Delta n_{12} - \Delta n_{23}) + \left(\frac{\Delta \phi_{12}}{2\pi} - \frac{\Delta \phi_{23}}{2\pi} \right) \right] \quad (33)$$

For clarity, the subscript of the parameter in the formula has been represented by a double number corresponding to the mark number at both ends of the baseline. Obviously, three phase-shift values need to be detected simultaneously to obtain the phase difference rate, that is, the one-dimensional double-base linear array as shown in Figure 3 needs to be adopted from the implementation method of measurement.

5. Difference Function of Path Difference on Unit Length

5.1 Decomposition of Functions

The representation of the phase difference rate based on multichannel detection of phase difference can be divided into the product as follow two items:

$$\frac{\partial \Delta}{\partial} = \iota_0 \cdot \Delta \quad (34)$$

The first item represents the circular angle per unit time when the carrier is moving at speed v and is undergoing the baseline length d :

$$\phi_{t0} = \frac{2\pi v}{d_i} = \frac{2\pi}{\Delta t_i} \quad (35)$$

The latter second term is called the difference term of path difference on the unit length:

$$\Delta^2 r_\lambda = (\Delta n_i - \Delta n_{i+1}) + \left(\frac{\Delta \phi_i}{2\pi} - \frac{\Delta \phi_{i+1}}{2\pi} \right) = \frac{\Delta r_i - \Delta r_{i+1}}{\lambda} \quad (36)$$

The difference terms $\Delta^2 r_\lambda$ of path difference on a unit length can be divided into the sum of two terms. The previous term is the difference of the integer of wavelength between two adjacent baselines:

$$\Delta^2 n_i = (\Delta n_i - \Delta n_{i+1}) \quad (37)$$

The latter term is the difference of phase difference between two adjacent baseline:

$$\Delta^2 \phi_i = \left(\frac{\Delta \phi_i}{2\pi} - \frac{\Delta \phi_{i+1}}{2\pi} \right) \quad (38)$$

That is:

$$\Delta^2 r_\lambda = \Delta^2 n_i + \frac{\Delta^2 \phi_i}{2\pi} \quad (39)$$

5.2 Change Rule

If $\Delta^2 r_\lambda$ is expressed as a function varying with the angle of arrival, the simulation calculation indicates that the previous term will always jump between 0 and 1, and the latter term $\Delta^2 \phi_i$ will jump within the range of $-1 < \Delta^2 \phi_i < 0.1$.

According to Matlab program, the theoretical calculation value of $\Delta^2 n_i$ is:

$$\Delta^2 n_i = [F\text{IX}(r_i / \lambda) - F\text{IX}(r_{i+1} / \lambda)] - [F\text{IX}(r_{i+1} / \lambda) - F\text{IX}(r_{i+2} / \lambda)] \quad (40)$$

Figure 4 shows the variation curve of the differential of the difference value of the number of wavelength at different angles of arrival. In order to keep the screen simple, the larger interval of the arrival angle is taken. The simulation shows that even if the interval of the angle is 0.01 degrees, $\Delta^2 n_i$ is still a jump back and forth between 0 and 1.

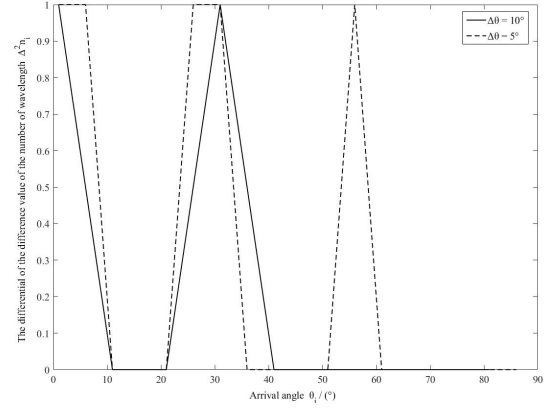


Figure 4. The differential of the difference value of the number of wavelength

The theoretical value of phase shift whose numerical value is less than π is:

$$\phi_i = 2\pi(r_i / \lambda - n_i) \quad (41)$$

Thereout, the theoretical calculation formula of differential of phase difference can be obtained:

$$\Delta^2 \phi_i = [(r_i / \lambda - n_i) - (r_{i+1} / \lambda - n_{i+1})] - [(r_{i+1} / \lambda - n_{i+1}) - (r_{i+2} / \lambda - n_{i+2})] \quad (42)$$

Figure 5 shows the variation curve of the differential of phase difference at different angle intervals.

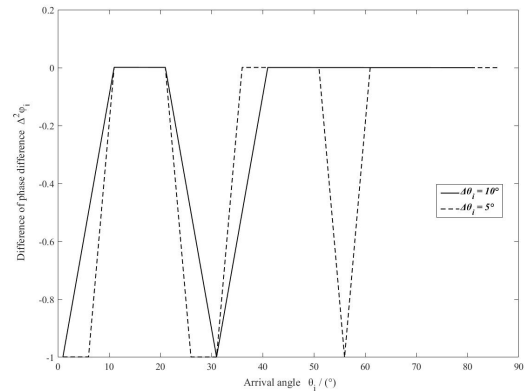


Figure 5. The differential of phase difference

5.3 Correction of Phase Jump

The analog calculation shows that the value of the differential term $\Delta^2 r_\lambda$ on the unit length is always less than 1.

As can be seen from the graph, the variation between the number of wavelength and the differential of phase differences is going to correspond to each other. If the preceding term has a jump change, the latter must also have a jump change, and the sum of the preceding and following terms is always to offset the value greater than 1 when the integral part of the differential item $\Delta^2 r_\lambda$ of path difference in unit length is greater than 1. Therefore, according to the numerical change rule that the sum of the two terms must offset the integral part greater than 1, If there is a jump on the differential of phase difference, then the measured data of phase difference can be corrected with the ± 1 .

The specific numerical simulation results are as follows:

When the absolute value of difference term of phase difference is $|\Delta\phi_{12} - \Delta\phi_{23}| < \pi$, directly take:

$$2\pi \cdot \Delta^2 \Delta\phi_i = (\Delta\phi_{12} - \Delta\phi_{23}) \quad (43)$$

When the difference term of phase difference is $(\Delta\phi_{12} - \Delta\phi_{23}) > 2\pi$, take:

$$2\pi \cdot \Delta^2 \Delta\phi_i = (\Delta\phi_{12} - \Delta\phi_{23}) - 2\pi \quad (44);$$

When it is $\pi < |\Delta\phi_{12} - \Delta\phi_{23}| < 2\pi$, take:

$$2\pi \cdot \Delta^2 \Delta\phi_i = 2\pi - |\Delta\phi_{12} - \Delta\phi_{23}| \quad (45)$$

That is, the piecewise equivalent function of the difference term of path difference on unit length is as follows:

$$\Delta^2 r_\lambda = \begin{cases} \Delta\phi_{12} - \Delta\phi_{23}, & |\Delta\phi_{12} - \Delta\phi_{23}| < \pi \\ (\Delta\phi_{12} - \Delta\phi_{23}) - 2\pi, & (\Delta\phi_{12} - \Delta\phi_{23}) > 2\pi \\ 2\pi - |\Delta\phi_{12} - \Delta\phi_{23}|, & \pi < |\Delta\phi_{12} - \Delta\phi_{23}| < 2\pi \end{cases} \quad (46)$$

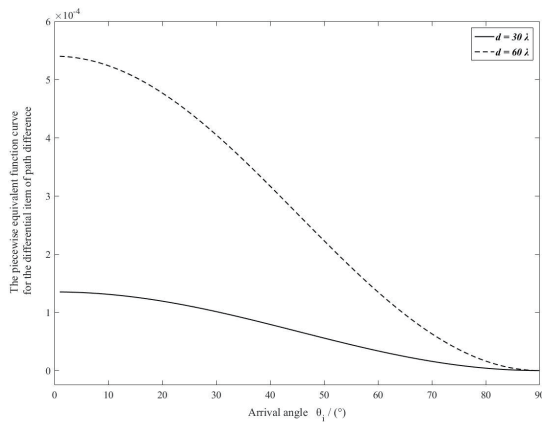


Figure 6. The piecewise equivalent function curve for the differential item of path difference

After modification is done in according to the numerical jump of the phase differential item, obtained piecewise equivalent function of the difference term of path difference on the unit length already has nothing to do with the computing of differential item of number of wavelength. The curve is shown in figure 6 shows that the range of the piecewise equivalent function for the differential item of path difference on the unit length is smooth continuous that is obtained only by measuring the phase difference.

5.4 Validation

Literature [16] has indirectly verified the correctness of the expression of phase difference rate based on multichannel phase difference measurement by using phase difference ranging method. In this chapter, the correctness of piecewise equivalent function of the differential item of path difference would be emphatically verified. The method is to use the theoretical value of the differential item of path difference on unit length

$$\Delta^2 r_\lambda = \frac{\Delta r_i - \Delta r_{i+1}}{\lambda} = \left(\Delta n_i + \frac{\Delta\phi_i}{2\pi} \right) - \left(\Delta n_{i+1} + \frac{\Delta\phi_{i+1}}{2\pi} \right) \quad (47)$$

Compared with the piecewise equivalent function obtained by phase difference correction, the relative calculation error is shown in figure 7. The simulation results show that the derived equation of the differential of path difference at present is only applicable to the shorter baseline length. When the radial distance is determined, the maximum usable baseline length can be estimated according to the following formula:

$$\frac{d}{\lambda} \leq \frac{18r}{2000} \quad (48)$$

Where: r represents the radial distance of the target.

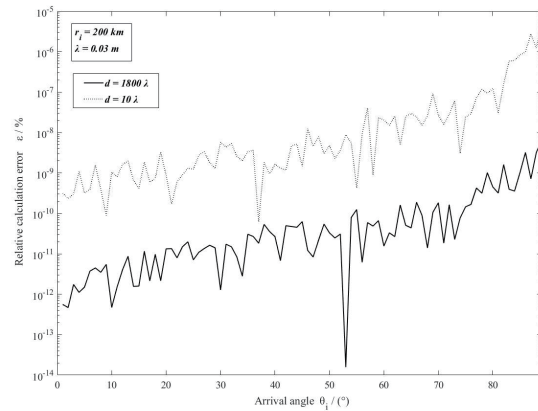


Figure 7. Relative calculation error of the differential item of path difference

6. Some Parameters Realized by the Phase Difference Measurement without Ambiguity

6.1 Relative Angular Velocity

6.1.1 Overview

In the airborne single-station passive positioning system, the observability of the positioning system can be increased and the positioning performance can be improved by introducing the observation information of angular velocity^[11, 21]. However, the angular velocity is a physical quantity of time derivative. Unless the gyroscope sensor is used, it usually needs to be obtained by indirect method. The difference method, or least square fitting method, or Kalman filter method, which estimates the change rate of angle by using angle measurement equipment to obtain angle sequence, requires that the angle observation value itself must be linear change during the sampling period, otherwise, the measurement accuracy of angle change rate will be difficult to be guaranteed^[22].

6.1.2 Basic Solution

Directly differential for direction finding formula based on phase differential measurement on a single basis, there is:

$$\omega \cos \theta = \frac{1}{d} \frac{\partial \Delta r}{\partial t} = \frac{\lambda}{2\pi d} \frac{\partial \Delta \phi}{\partial t} \quad (49)$$

Where: ω is the angular velocity.

After the transposition arrangement, by substituting the phase difference rate based on the multichannel phase difference detection into (49), we obtain:

$$\omega = \frac{\lambda}{2\pi d \cos \theta} \frac{\partial \Delta \phi}{\partial t} = \frac{\lambda v}{d^2 \cos \theta} \left[(\Delta n_1 - \Delta n_2) + \left(\frac{\Delta \phi_1}{2\pi} - \frac{\Delta \phi_2}{2\pi} \right) \right] \quad (50)$$

Furthermore, the non-fuzzy solution of the phase difference rate is substituted into, and the relative angular velocity calculation formula based on measurement of azimuth angle and the difference of non-fuzzy phase difference is obtained:

$$\omega = \frac{\lambda v}{d^2 \cos \theta} \Delta^2 r_\lambda \quad (51)$$

6.1.3 Error

In order to facilitate the error analysis, the non-fuzzy solution is first reduced to a form that contains the difference value of the integer of wavelength, and it is regarded as a constant:

$$\omega = \frac{\lambda v}{d^2 \cos \theta} \left[(\Delta n_1 - \Delta n_2) + \left(\frac{\Delta \phi_1}{2\pi} - \frac{\Delta \phi_2}{2\pi} \right) \right] \quad (52)$$

Partial differential to each phase difference is:

$$\frac{\partial \omega}{\partial \Delta \phi_1} = \frac{\lambda v}{2\pi d^2 \cos \theta} \quad (53)$$

$$\frac{\partial \omega}{\partial \Delta \phi_2} = -\frac{\lambda v}{2\pi d^2 \cos \theta} \quad (54)$$

$$\frac{\partial \omega}{\partial \theta} = -\frac{\lambda v \sin \theta}{d^2 \cos^2 \theta} \left[(\Delta n_1 - \Delta n_2) + \left(\frac{\Delta \phi_1}{2\pi} - \frac{\Delta \phi_2}{2\pi} \right) \right] \quad (55)$$

$$\frac{\partial \omega}{\partial v} = \frac{\lambda}{d^2 \cos \theta} \left[(\Delta n_1 - \Delta n_2) + \left(\frac{\Delta \phi_1}{2\pi} - \frac{\Delta \phi_2}{2\pi} \right) \right] \quad (56)$$

According to the error estimation theory, the measurement error of relative angular velocity caused by phase difference, angle and velocity is:

$$\sigma_r = \sqrt{\left(\frac{\partial \omega}{\partial v} \sigma_v \right)^2 + \sum_{i=1}^2 \left(\frac{\partial \omega}{\partial \Delta \phi_i} \sigma_{\phi_i} \right)^2 + \left(\frac{\partial \omega}{\partial \theta} \sigma_{\theta} \right)^2} \quad (57)$$

Where: σ_v is the root mean square value of velocity measurement error, and takes $\sigma_v = 0.1 \text{ m/s}$ when analyzing and calculating; σ_{ϕ} is the root mean square value of the measurement error of phase difference, unit is radian, and takes $\sigma_{\phi} = 5\pi/180$ that can be reached by general engineering measurement; σ_{θ} is the root mean square value of the angle measurement error, in radian, and takes $\sigma_{\theta} = 1^\circ \pi/180$.

Figure 8 shows the angular velocity measurement error at different baseline lengths. It can be seen from this that the measurement accuracy less than 3 mrad/s can be achieved within a larger angle of arrival if the ratio between baseline and wavelength is large enough.

The parameters used in the simulation calculation are: the target distance is 300 kilometers; Airborne platform mobility speed 300m/s; Wave length 0.03 m.

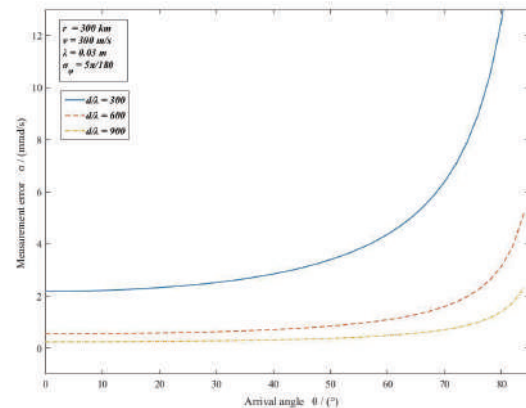


Figure 8. the angular velocity measurement error at different baseline lengths

6.1.4 Summary

As far as the analysis process is concerned, the angular velocity calculation method based on multichannel phase difference measurement is not only high accuracy but also real-time. Because it is only requirement to directly measure the phase difference, there is no need to maintain linear variation for the angle measurement.

6.2 Radial Acceleration

6.2.1 The Introduction

Based on the principle of kinematics, radial acceleration can be used for passive localization, and radial acceleration information can be used to reduce the limitation for observability of observer motion, and to improve the convergence speed of positioning error and positioning accuracy to some extent^[11].

However, in the engineering application, according to the existing research analysis, radial acceleration seems to be difficult to detect. The difficulty of detection in the time domain is that the high precision of time measurement is need, which is about 1/10 nanosecond. However, in the frequency domain, most radar signals are pulses with very short duration and the signal frequency changes are difficult to detect. Therefore, it is difficult to obtain accurate parameter estimation from a single pulse signal, which requires long time accumulation for signals and the use of impulse coherence^[1]. In addition, although the radial acceleration of the target relative observer can be obtained by measuring the carrier frequency change rate of incoming waves or the pulse repetition rate, in fact the frequency change rate of intra-pulse phase modulation signal cannot directly characterize the Doppler frequency shift change rate^[23].

Different from the existing method to obtain radial acceleration by analyzing the phase parameters of the signal based on signal modeling, in this paper, by using the functional relation between phase shift and frequency shift, and by using the mathematical definition of radial acceleration, the analytic expression of radial acceleration only based on phase difference measurement can be obtained by carrying on the quadratic differential to the function between distance and phase shift. On the basis of this, a non-fuzzy phase difference detection method for airborne radial acceleration is presented according to the method of non-fuzzy detection of phase difference rate.

6.2.2 Derivation

Use the relation between radial distance change rate and phase shift change rate:

$$\frac{\partial r_i}{\partial t} = \frac{\lambda}{2\pi} \frac{\partial \phi_i}{\partial t} \quad (58)$$

By the mathematical definition of radial acceleration, after differentiating radial velocity, we can obtain:

$$a_{ri} = \frac{\partial^2 r_i}{\partial t^2} = \frac{\lambda}{2\pi} \frac{\partial^2 \phi_i}{\partial t^2} \quad (59)$$

The radial acceleration can be obtained by substituting the expression (29) of the phase shift change rate based on the measurement of phase difference into (59):

$$a_r = \frac{\lambda}{2\pi} \frac{\partial}{\partial t} \left[\frac{2\pi v}{d_1} \left(\Delta n_1 + \frac{\Delta \phi_1}{2\pi} \right) \right] = \frac{\lambda v}{2\pi d_1} \frac{\partial \Delta \phi_1}{\partial t} \quad (60)$$

Then, the expression (33) of the phase difference rate based on the phase difference measurement is substituted into, and there is:

$$a_r = \lambda \left(\frac{v}{d} \right)^2 \left[(\Delta n_1 - \Delta n_2) + \left(\frac{\Delta \phi_1}{2\pi} - \frac{\Delta \phi_2}{2\pi} \right) \right] \quad (61)$$

By substituting the non-fuzzy solution of the phase difference rate, the calculated formula of radial acceleration based on the difference measurement of phase difference without obscure can be obtained:

$$a_r = \lambda \left(\frac{v}{d} \right)^2 \Delta^2 r_\lambda \quad (62)$$

Obviously, radial acceleration is the acceleration on the difference length of the path difference, that is, differential acceleration.

6.2.3 Estimation of Detection Accuracy

According to the error estimation theory, the error of acceleration measurement caused by phase difference, velocity and baseline spacing is:

$$\sigma_{ar} = \sqrt{\sum_{i=1}^2 \left(\frac{\partial a_r}{\partial \Delta \phi_i} \sigma_\phi \right)^2 + \left(\frac{\partial a_r}{\partial v} \sigma_v \right)^2 + \left(\frac{\partial a_r}{\partial d} \sigma_d \right)^2} \quad (63)$$

Where: σ_v is the root mean square value of velocity measurement error, and $\sigma_v = 0.1m/s$ is taken when analyzing and calculating; σ_ϕ the root mean square value of the measurement error of phase difference, unit is radian, and $\sigma_\phi = (2 \sim 10)\pi/180$ can be reached for the general engineering measurement; $\sigma_d = 0.1m$ the root mean square value of the measurement error of baseline spacing.

Partial differential of each observed quantity is:

$$\frac{\partial a_r}{\partial \Delta \phi_1} = \frac{\lambda}{2\pi} \left(\frac{v}{d} \right)^2 \quad (64)$$

$$\frac{\partial a_r}{\partial \Delta \phi_2} = -\frac{\lambda}{2\pi} \left(\frac{v}{d} \right)^2 \quad (65)$$

$$\frac{\partial}{\partial v} = \frac{1}{d} \left[(\Delta N_1 - \Delta N_2) + \left(\frac{\Delta \phi_1}{2\pi} - \frac{\Delta \phi_2}{2\pi} \right) \right] \quad (66)$$

$$\frac{\partial}{\partial d} = -\frac{1}{d} \left[(\Delta N_1 - \Delta N_2) + \left(\frac{\Delta \phi_1}{2\pi} - \frac{\Delta \phi_2}{2\pi} \right) \right] \quad (67)$$

It can be seen directly from the each measurement error terms that the measurement error is directly proportional to the flight speed and signal wavelength and inversely proportional to the baseline length.

Figure 9 shows the measurement error at different baseline lengths, from which it can be seen that the measurement error of acceleration is less than $1m/s^2$ as long as the baseline is greater than 100 wavelength when the speed of fighter plane is 100m/s. The effect on measurement error is not very big if σ_d is less than 1 meter.

The simulation results show that the influence of velocity on the measurement error is relatively large. If the aircraft's flight speed is higher, the obtained acceleration will be imprecise.

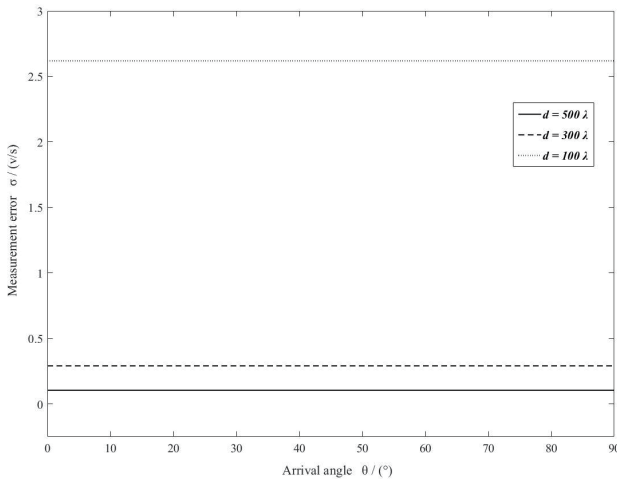


Figure 9. Measurement error at different baseline lengths

6.2.4 Summary

With the development of electronic warfare technology, more and more radars adopt uncertain signal forms, which will complicate the estimation problem of radial accel-

eration. However, the method proposed in this chapter for direct detection of radial acceleration based on phase interference can effectively simplify the measurement process, and the obtained analytical solution of airborne radial acceleration does not need to estimate the carrier rate or the pulse repetition rate of the incoming wave. But the error analysis shows that the measurement accuracy of radial acceleration is proportional to the baseline length of the receiving array. In order to obtain higher measurement accuracy, the baseline length must be increased. But, the phase ambiguity problem must be solved effectively when using long baseline measures the phase difference. There is no doubt that the method of non-fuzzy phase difference detection provides technical support for long baseline phase measurement and real-time detection of observed quantity on airborne platform.

6.3 Change Rate of Doppler Shift

6.3.1 Overview

The change rate of Doppler frequency reflects the radial acceleration information of the moving target relative to the observation station. It is of great significance to obtain the change rate of Doppler frequency for the target localization and the estimation of the motion state. But the change rate of Doppler is very weak, especially for radar pulses. Since the pulse duration is generally very short, it is very difficult to achieve high precision measurement with a single pulse when the SNR and sampling points are fixed.

In general, the main method to detect the change rate of Doppler is that by estimating the frequency change of the received signal obtains the change rate of Doppler frequency based on the principle that the change rate of Doppler frequency is mathematically the same as the change rate of carrier frequency of the signal^[24-25]. That is, the change rate of Doppler can be measured indirectly through the measured radiation frequency. However, these estimation algorithms are not only related to the received signal modulation, but also more complex.

One of the main methods to detect the change rate of Doppler proposed in recent years is the application of digital signal processing technology in digital receivers. By using the phase-coherent characteristics between pulse carrier frequencies makes multiple pulses form a continuous signal. From this, the effective observation time of the signal is equivalently extended. The least squares algorithm based on phase difference^[26-27] can be used to obtain higher measurement accuracy. However, this method requires high signal-to-noise ratio (SNR) and must ensure that the measurement of phase does not appear blurred.

6.3.2 Deduction

According to the existing analysis, the change rate of frequency shift measured based on the phase difference rate is:

$$\frac{\partial f_d}{\partial t} = \frac{v^2}{d^2} [(\Delta n_1 - \Delta n_2) + (\Delta \phi_1 - \Delta \phi_2) / 2\pi] \quad (68)$$

On the substitution of the differential item of path difference on the unit length into Eq.(68), there is:

$$\frac{\partial f_d}{\partial t} = \frac{v^2}{d^2} \Delta^2 r_\lambda \quad (69)$$

According to the method in the previous section, the change rate of Doppler is the acceleration on the difference length of the path difference based on the unit wavelength, or the ratio of the difference acceleration to the wavelength.

6.3.3 The Error Analysis

According to the error estimation theory, the measurement error of the change rate of Doppler caused by phase difference and velocity is:

$$\sigma_f = \sqrt{\left(\frac{\partial f_d}{\partial v} \sigma_v \right)^2 + \sum_{i=1}^2 \left(\frac{\partial f_d}{\partial \Delta \phi_i} \sigma_{\phi} \right)^2} \quad (70)$$

Where: σ_v is the root mean square value of velocity measurement error, and $\sigma_v = 0.1m/s$ is taken when analyzing and calculating; σ_{ϕ} the root mean square value of the measurement error of phase difference, in radian, and takes $\sigma_{\phi} = \pi/90$.

It could be established:

$$F_d = \frac{v^2}{d^2} [(\Delta n_1 - \Delta n_2) + (\Delta \phi_1 - \Delta \phi_2) / 2\pi] \quad (71)$$

Each partial differential of phase difference and velocity is:

$$\frac{\partial F_d}{\partial \Delta \phi_1} = \frac{v^2}{2\pi d^2} \quad (72)$$

$$\frac{\partial F_d}{\partial \Delta \phi_2} = -\frac{v^2}{2\pi d^2} \quad (73)$$

$$\frac{\partial F_d}{\partial v} = \frac{2v}{d^2} [(\Delta n_1 - \Delta n_2) + (\Delta \phi_1 - \Delta \phi_2) / 2\pi] \quad (74)$$

From the expression of measurement error, it can be seen that the measurement error is directly proportional to the movement of the airborne platform and inversely proportional to the baseline length. Obviously, the baseline length must be increased to reduce the measurement error. Figure 10 shows the measurement error of the change rate of Doppler at different baseline lengths. It can be seen that the measurement error of the change rate of Doppler can be reduced to a few Hertz after the ratio of baseline to wavelength is greater than 500.

The parameters used in the simulation calculation have been indicated in the figure.

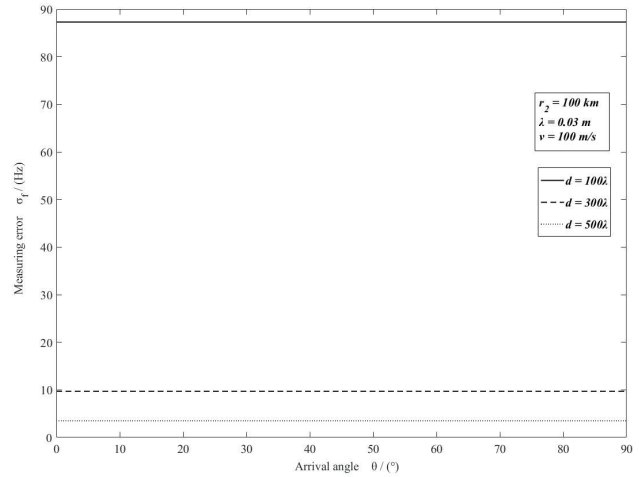


Figure 10. The measurement error of the change rate of Doppler at different baseline lengths

6.3.4 Summary

Using the method for detecting the change rate of Doppler based on multichannel phase difference measurement, not only can the change rate of Doppler be obtained in real time, but also the theoretical analysis shows that as long as the baseline is long enough, the measurement error for detecting the change rate of Doppler can be controlled within a few Hertz.

6.4 Change Rate of Time Difference

6.4.1 Overview

The introduction of time difference as well as change rate in single-station passive location will help improve the positioning accuracy, and the passive location method based on time difference as well as change rate has the advantage of being suitable for both wide and narrow band signals^[28-31]. However, in general, the change rate of time difference is a physical quantity which is

indirectly obtained through continuous measurement of time series, so the sampling detection method will be difficult to be applied to real-time detection of moving target by moving platform. In fact, in the case of short baseline applications for airborne single-station, the measurement of time difference is also a very difficult thing.

This chapter theoretically proves that the time difference as well as change rate on airborne station can be obtained indirectly through the phase difference measurement. In fact, the expression of time difference based on phase difference detection can be solved by using the location equation of phase difference and time difference, and the change rate of time difference based on phase difference detection can be obtained by differentiating and using the functional relation between phase shift and frequency shift. The preliminary error analysis shows that the detection of the change rate of time difference based on phase difference measurement can have a higher measurement accuracy because the magnitude of the light speed is very large in the denominator.

6.4.2 Time Difference Detection Based on Phase Difference Measurement

If two equation, the location equation of the phase differential and the time difference, are combined:

$$\Delta r = r_1 - r_2 = \lambda \left(n_1 - n_2 + \frac{\phi_1 - \phi_2}{2\pi} \right) \quad (75)$$

$$\Delta r = r_1 - r_2 = v_c \Delta t \quad (76)$$

The time difference estimation formula based on the phase difference detection can be solved out:

$$\Delta t = \frac{\lambda}{v_c} \left(\Delta n + \frac{\Delta \phi}{2\pi} \right) \quad (77)$$

The time difference measurement error caused by phase difference measurement is:

$$\frac{\partial \Delta t}{\partial \Delta \phi} = \frac{\lambda}{2\pi v_c} \quad (78)$$

The measurement error curve is shown in figure 11. Since it is inversely proportional to the speed of light with a large order of magnitude, the measurement error based on the phase difference detection is about 10ns.

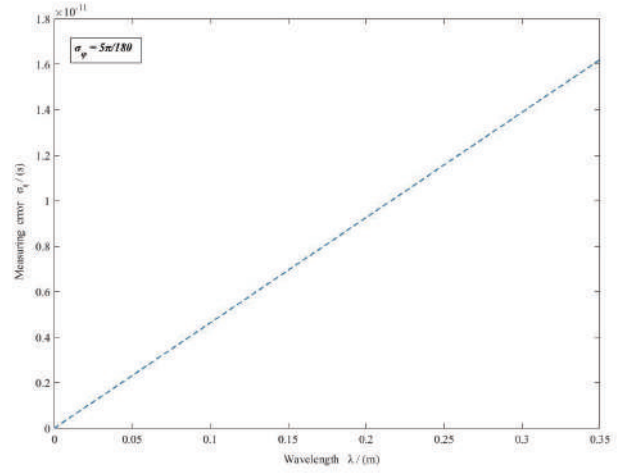


Figure 11. Time difference measurement error

6.4.3 Detection of Change Rate of Time Difference Based on Phase Difference Measurement

Furthermore, after differentiating both sides of the time difference expression based on the phase difference detection with respect to time, we have:

$$\frac{\partial \Delta t}{\partial t} = \frac{\lambda}{2\pi v_c} \frac{\partial \Delta \phi}{\partial t} \quad (79)$$

By using the relationship (33) of the phase difference rate based on the phase difference measurement, the change rate of time difference based on the phase difference detection can be obtained:

$$\frac{\partial \Delta t}{\partial t} = \frac{\lambda v}{v_c d} \left[(\Delta n_1 - \Delta n_2) + \left(\frac{\Delta \phi_1}{2\pi} - \frac{\Delta \phi_2}{2\pi} \right) \right] \quad (80)$$

Where: v_c is the speed of light.

Further, the non-fuzzy solution of the phase difference rate was substituted into, as follows:

$$\frac{\partial \Delta t}{\partial t} = \frac{\lambda v}{v_c d} \Delta^2 r_\lambda \quad (81)$$

6.4.4 Measurement Accuracy of the Change Rate of Time Difference

For clear writing, set:

$$F_\phi = \frac{\lambda v}{v_c d} \left[(\Delta n_1 - \Delta n_2) + \left(\frac{\Delta \phi_1}{2\pi} - \frac{\Delta \phi_2}{2\pi} \right) \right] \quad (82)$$

According to the error estimation and synthesis theory, the error components in the calculation formula of the

change rate of time difference, which can be obtained by partial differentiation of each parameter, are:

$$\frac{\partial F_{\phi}}{\partial \Delta \phi_1} = \frac{\lambda v}{2\pi d v_c} \quad (83)$$

$$\frac{\partial F_{\phi}}{\partial \Delta \phi_2} = -\frac{\lambda v}{2\pi d v_c} \quad (84)$$

$$\frac{\partial F_{\phi}}{\partial v} = \frac{\lambda}{d v_c} \left[(\Delta n_1 - \Delta n_2) + \frac{(\Delta \phi_1 - \Delta \phi_2)}{2\pi} \right] \quad (85)$$

The absolute measurement error caused by phase difference and velocity is:

$$\sigma_t = \sqrt{\left(\frac{\partial F_{\phi}}{\partial v} \sigma_v \right)^2 + \sum_{i=1}^2 \left(\frac{\partial F_{\phi}}{\partial \Delta \phi_i} \sigma_{\phi} \right)^2} \quad (86)$$

Where: σ_v is the root mean square value of velocity measurement error, and $\sigma_v = 0.1 \text{ m/s}$ is taken when analyzing and calculating; σ_{ϕ} the root mean square value of the measurement error of phase difference, in radian, and the general engineering measurement can reach $\sigma_{\phi} = (2 \sim 10)\pi / 180$.

From the perspective of the error component, both the increase of baseline length and the decrease of movement speed can reduce the measurement error, but limited by the current technical level, the increase of baseline length is very limited. Figure 12 shows the measurement error at different flight speeds. Obviously, low speed can obtain better measurement accuracy.

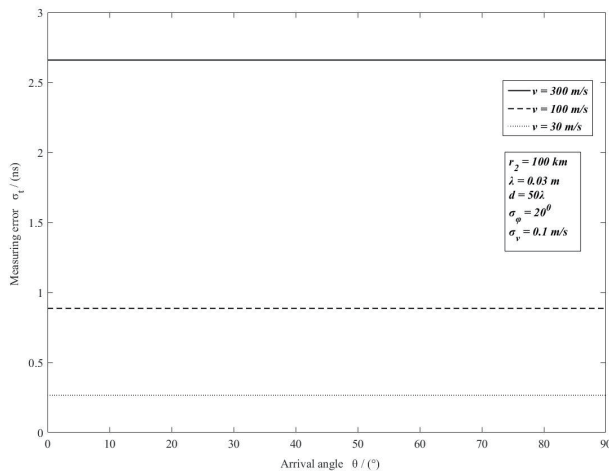


Figure 12. The measurement error at different flight speeds

6.4.5 Summary

Although the technology of short baseline time difference measurement has made great progress, since the time difference at both ends of the short baseline is very small in the application of the airborne short baseline, therefore, it is difficult to realize real-time detection of time difference and its change rate if we don't get the time series through the continuous flight of the carrier platform according to the existing technology of time difference measurement.

Obviously, only the phase difference measurement method is suitable for short baseline application at present, and it is a fairly mature measurement technology. If the exploration and research in this chapter is correct, it means that the phase difference measurement technology can be used to realize real-time detection for the change rate of time difference on the airborne platform. However, the research in this chapter is only a pure theoretical analysis at present, and how to be applied remains to be further studied.

One of the problems is that the phase difference measurement method can only be applied to detect narrow-band signals, which is obviously inconsistent with the characteristics that the time difference and its change rate can be applied to broadband signals. This in fact means that the method of getting the change rate of time difference based on the phase difference measurement may not be suitable for the detection of broadband signals.

7. Conclusion

The author's research results show that, based on the multichannel phase difference measurement and only using the measurement value of phase difference, the phase difference rate can be directly obtained by using the differential of the difference value of integer of wavelength and the jump rule of the differential of phase difference under the condition of the unknown the difference value of integer of wavelength.

The author's research results undoubtedly provide a strong technical support for the practical engineering design related to the phase measurement, the most important result is that it lays a very important foundation for the engineering application of phase difference localization. The phase detection method without obscure based on the phase difference rate can indirectly realize the phase difference location without obscure.

Before that, since there is the period ambiguity in phase difference measurement, the observed quantity itself contains the unknown difference value of integer of wavelength in the observation process. And the unknown parameter also changes with the change of geometric ob-

servation. Therefore, the positioning equation based on the phase difference measurement is not solvable directly from the mathematical equation.

Reference

- [1] Fucheng Guo, Xingjiang Jia. A Single Observer Passive Localization Method Using Phase Difference Changing Rate Only and Its Error Analysis[J]. *Acta Aeronautica Et Astronautica Sinica*, 2009, 30(6): 1090-1095.
- [2] Qiang Wang, Danxing Zhong, Fucheng Guo, Xinpu Deng, Yiyu Zhou. A single moving observer passive localization method using LBI phase difference change rates only[J]. *Signal Processing*, 2009, 25(8A): 566-569.
- [3] Weiqiang Zhu, Pei-kang Huang, Qin Ma. Location method for phase difference rate of change with single-observer[J]. *Systems Engineering and Electronics*, 2008, 30(11): 2108-2111.
- [4] Deng-cai Huang, Min Ding. Introduction to Passive Location Using Phase Rate of Change[J]. *Modern Radar*, 2007, 29(8): 32-34+51.
- [5] Yuehui Shan, Zhongkang Sun, Fukan Huang. Research on Single Observer-Passive Location Technology Based on Method of Phase Difference Rate of Change[J]. *Journal of National University of Defense Technology*, 2001, 23(16): 74-77.
- [6] Wenjian Si, Dianfa Ping, Feng Su, Peihong Zhao. Study on Technology of Airborne Passive Location Based on Phase Rate of Change[J]. *Ship Electronic Engineering*, 2010, 30(4): 76-79.
- [7] Guoqing Zhao. Radar countermeasures[M]. Xi'an university of electronic science and technology press, 1999.
- [8] Huashan Ma. Project implementation of design and direction finding algorithm for a direction finding antenna array using phase interferometer with three-baseline[J]. *Telecommunications research*, 2011(1): 28-33.
- [9] Xuejin Jiang, Xia Gao, Yang Shen. Design of Multi-Baseline Interferometer[J]. *Electronic Information Warfare Technology*, 2008, 23(4): 39-45.
- [10] Zhiyu Qu, Xicai Si. Direction Finding Method of Wideband Passive Radar Seeker Based on Virtual Baseline[J]. *Journal of Projectiles, Rockets, Missiles and Guidance*, 2007, 27(4): 92-95.
- [11] Zhongkang Sun. Passive location and tracking technology by single observer[M]. Beijing: National defense industry press, 2008.
- [12] Dengcai Huang, Min Ding. Introduction to Passive Location Using Phase Rate of Change[J]. *Modern Radar*, 2007, 29(8): 32-34+51.
- [13] Weiqiang Zhu, Peikang Huang, Qin Ma. Location method for phase difference rate of change with single-observer[J]. *Systems Engineering and Electronics*, 2008, 30(11): 2108-2111.
- [14] Yaowei Xu, Zhongkang Sun. The passive location for the moving radiation source by using phase difference rate[J]. *Systems Engineering and Electronics*, 1999, 21(8): 7-8.
- [15] T. Yu, Airborne passive localization method based on Doppler- phase interference measurement. In: I. Padron, Ed., *Recent Interferometry Applications in Topography and Astronomy*, InTech Publisher, 2012: 133-168.
- [16] Yu Tao. Method Obtaining Phase-Difference Rate by Multichannel Phase Difference Detection on Airborne Platform[J]. *Journal of Aerospace Science and Technology*, 2013, 1(1): 1-5.
- [17] Wang Yong, Ye Bin, Xie Chunsheng. New time difference direction finding method[J]. *Electronic Warfare Technology*, 1995(3): 1-7.
- [18] Gong Yu. Time difference direction finding method[J]. *Electronic Warfare Technology*, 1994(2): 18-23.
- [19] Shao Jianhua. Analysis of direction finding accuracy for short baseline time difference[J]. *Aerospace Electronic Warfare*, 1998(1): 16-18.
- [20] Shao Jianhua. Technology system and application prospect of short baseline time difference direction finding[J]. *Aerospace Electronic Warfare*, 1997(4): 23-25.
- Technology system and application prospect of short baseline time difference direction finding
- [21] Zeng Que. Measuring method of phase difference rate[J]. *Aerospace Electronic Warfare*, 2003(3): 36-38.
- [22] Guo Hui, Ma Baohong, Hou Qingyu. Measurement method of angle changing rate in single-station passive location[J]. *Aerospace Electronic Warfare*, 2011, 27(3): 30-32, +57.
- [23] Li Hong Qin Yuliang, Li Yanpeng Wang, Hong qiang, Li Xiang. A Phase Compensation Based Algorithm for Doppler Frequency Rate Estimation from BPSK Coherent Pulse Train[J]. *Journal of Electronics & Information Technology*, 2010, 32(9): 2156-2160.
- [24] Gaoying Zhou. Study on the dual station passive location algorithm based on the difference value of Doppler Frequency rate [D]. Nanjing university of aeronautics and astronautics, 2012.
- [25] Zhan Gmin. Study on measurement technology of Doppler Frequency rate in passive location of single

- star[D].University of national defense science and technology, 2009.
- [26] Junhu Wang, Xinpu Deng. Measurement method of Doppler Frequency Rate of Coherent Pulse signal[J]. Aerospace Electronic Warfare, 2005, 21(2-2): 41-43+50.
- [27] Daowan Fong, Yiyu Zhou, Zonghua Li. A Fast and Accurate Estimator for Doppler Rate-of-Change with the Coherent Pulse Train[J]. Signal Processing, 2004, 20(2-1): 40-43.
- [28] Xingjiang Jia, Fucheng Guo, Yiyu Zhou. Passive Localization Based on Short Time TDOA Sequence[J]. Acta Aeronautica Et Astronautica Sinica, 2011, 48(2): 291-298.
- [29] Ying Wen, Donghai Li, Dexiu Hu. A Method of Single Observer Passive Location Based on Time Delay Rate[J]. Command Information System and Technology, 2011, 2(1): 27-30+48.
- [30] Huo Guang, Donghai Li. Approach of Airborne Single -station Passive Locating for an Emitter with Fixed Wideband[J]. Fire Control Radar Technology, 2012, 41(4): 31-35.
- [31] Ying Wen, Donghai Li, Dexiu Hu. A Single Observer Passive Localization Method for Wideband Signal Based on Time Delay and Time Delay Rate[J]. Electronic Warfare Technology, 2012, 27(2): 14-17.

**ARTICLE****A Novel Image Encryption Scheme Based on Reversible Cellular Automata****Zeinab Mehrnahad Ali Mohammad Latif***

Computer Engineering Department, Yazd, Iran

ARTICLE INFO*Article history*

Received: 27 July 2019

Accepted: 29 September 2019

Published Online: 18 October 2019

Keywords:

Cryptography

Cellular automata

Reversible cellular automata

Image encryption

Image scrambling

Image substituting

ABSTRACT

In this paper, a new scheme for image encryption is presented by reversible cellular automata. The presented scheme is applied in three individual steps. Firstly, the image is blocked and the pixels are substituted by a reversible cellular automaton. Then, image pixels are scrambled by an elementary cellular automata and finally the blocks are attached and pixels are substituted by an individual reversible cellular automaton. Due to reversibility of used cellular automata, decryption scheme can reversely be applied. The experimental results show that encrypted image is suitable visually and this scheme has satisfied quantitative performance.

1. Introduction

With development of communication, computer networks and digital multimedia, information security has become important. This development has some problems such as illegal copy and distribution of digital media. To solve this problem, some methods have been proposed^[1-2].

Cryptography is one of the most common methods for information security. It derived from reversible mathematical operation and a set of rule-based calculations called algorithms for generating key of cryptography. Mathematical operations and keys are used to transform multimedia contents in ways that are hard to decryption. The encryption key is considered as the main element in

cryptography, so that without the key, even with knowing the algorithm, decryption is impossible^[3]. Digital images are greatly used in multimedia applications recently. These images contain private information in business, military, political, medical and the privacy of visual information is also important^[2].

Text encryption algorithms are not suitable for images since these methods require a long computational time and power. Also, images are different from text due to dependency of its pixels. Therefore, special encryption methods are presented for image encryption^[4].

Substitution and scrambling are main image encryption methods. Scrambling changes, the arrangement of pixels in the image. In this method, the position of the pixels

**Corresponding Author:*

Ali Mohammad Latif,

Computer Engineering Department, Yazd, Iran;

Email: alatif@yazd.ac.ir

changed and the encrypted image is obtained. At the destination, according to a recursive process, the initial arrangement of the pixels is obtained^[5-7].

In substitution, the value of the pixels is changed by logical and computational operations and then in destination reverse encryption method is performed to retrieve pixel values^[8-10].

Cellular Automata (CA) with its inherent characteristics such as the possibility of parallel processing, uniformity, unpredictability of behavior and simple implementation is suitable for image encryption. CA were introduced in 1940's by Von Neumann^[11]. After introducing of CA, extensive studies have been done on it. In recent years, CA have been used in cryptography^[12-14], image processing^[15] and information security^[16-17].

In 2008, Ruisong introduced a method for image encryption using CA. He first generated a sequence of random numbers using CA. Then, he scrambled the image using these^[18].

In 2013, Fasel-Qadir et al. proposed digital image scrambling based on two dimensional cellular automata. He used CA for random number generator^[19]. It should be noted that image scrambling techniques do not have high security due to the lack of histogram changes.

In 2012, Jin introduced a method for image cryptography using CA^[20]. It was a simple image encryption method based on Elementary Cellular Automata (ECA). State attractors generated by ECAs under certain evolution rules perform the encryption function to transform pixel values of image, and the encrypted image is obtained. This method has a periodic behavior. Periodicity means a series of successive rules can be used in rotational way to achieve the original image.

In 2013, Abdo proposed a method based on pixel substitution. In this method, a linearly array of cells with a periodic behavior are generated by CA^[21]. In this method loops of recursive rules are formed, and it used to encrypt and decrypt image periodically. In both of above methods, due to the periodicity of the algorithm, there is the possibility of attack and image decryption.

In 2013, Wang proposed a method based on pixel scrambling and substitution^[22]. In the scrambling section, reversible CA were used. Substitution was performed only on low-value 4 bits. Therefore, the chance of randomness in this method is less and not suitable for encryption.

In 2014, Mohamed presented a blocking method for cryptography of the image using recursive CA^[23]. In this method by using reversible CA, a pseudorandom permutation is first constructed, and then it injected into a parallelizable encryption schema that act on the different blocks of a digital image independently. This method per-

forms well on multi-processor platforms and need powerful hardware implementation.

In this paper, image cryptography is provided using both elementary CA and a reversible CA. In this method the combination of substitution and scrambling has been used. We use two reversible CA for substitution and an elementary CA for scrambling; so the proposed structure consists of three automata and image cryptography is performed in three steps. It should be noted that the proposed structure is reversible and by applying each step reversely, decryption is performed.

2. Cellular Automata

CA is a mathematical model for discrete dynamic systems consisting of a number of cells. These cells form a network that can have different dimensions. CA has four components in the form of $CA = \{C, S, V, F\}$. The component C indicates the automata cell and S indicates the cell state. In most applications, the cells have two states of zero and one. The component V indicates the dimensions of the automata and the type of neighborhood. The component F indicates the rules for the transfer of CA^[24].

A sample of CA including one-dimensional neighborhoods and a periodic boundary state with the transfer rule 30 is shown in Table 1. The first column shows eight possible states for cells with radius neighborhood 1 and second column shows the next state of each cell. The rule number 30 is placed binary in the second column.

Table 1. Elementary CA with rule = 30

$S_{t,j-1}^{t-1}, S_{t,j}^{t-1}, S_{t,j+1}^{t-1}$	$S_{t,j}^t$
000	0
001	1
010	1
011	1
100	1
101	0
110	0
111	0

In Table 2, the initial input vector of the automata is considered as [0 1 1 0 1 0 1 1]. To apply rule number 30 and 1-D neighborhood to determine the next state, the following procedure is applied. Given the 1-D neighborhood, the first three pixels^[0 1 1] are selected. According to the rule 30, the next state is considered 1. Similarly, for the next three pixels, the rule^[1 1 0] is applied and the next state of the cell becomes 0. This process continues for the other pixels. For the first and last pixels, the periodic boundary state is considered. The general trend up to 2 steps is shown in

Table 2.

Table 2. Example of CA with rule = 30

Input vector	01101011							
1-d neighborhood	101	011	110	101	010	101	011	100
Next state	0	1	0	0	1	0	1	0
Output vector	01101011							
Of step 1	01001010							
1-d neighborhood	001	010	100	001	010	101	010	100
Next state	1	1	1	1	1	0	1	1
Output vector	01101011							
Of step 2	01001010							
	11111011							

3. Reversible Cellular Automata

CA are not inherently reversible, so that only a limited number of rules are reversible. In order to have a proper cryptography algorithm, the mathematical operation should be reversible. Cryptography using these limited rules does not have the complement security. Therefore, we decided to use a reversible CA in this study.

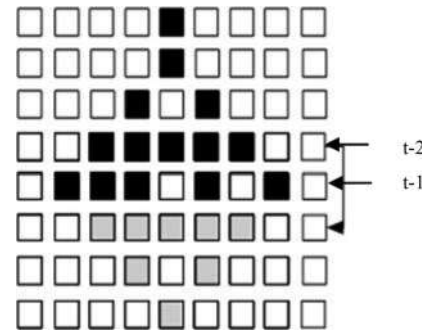
In reversible CA, the new state of a cell is determined not only by the cell itself and its neighbors one step back but also by the cell itself two steps back (time(t-1) and (t-2)) [27-28]. For each cell of two step back (time (t-2)), there are two states of zero and one. In addition, for each cell and its neighbors one step back (time (t-1)) for 1-D neighborhoods, eight states can be defined. These two times are shown in Table 3. According to the rule number, we can determine the cell state for time t. In this method, two rules are considered for automata ($R1$ and $R2=2^n-R1-1$). This is shown in the second column of table 3 for two rules of 30 and 225.

Table 3. Reversible CA with $R1 = 30$ and $R2=225$

$S_{i,j-1}^{t-1} S_{i,j}^{t-1} S_{i,j+1}^{t-1}$	$S_{i,j}^t$	
	$S_{i,j}^{t-2=1}$	$S_{i,j}^{t-2=0}$
	($R1=30$)	($R2=225$)
000	0	1
001	1	0
010	1	0
011	0	1
100	1	0
101	0	1
110	0	1
111	0	1

An example of reversible CA with rule 30 is shown in

Figure 1. The first row is the input vector and the second row is repetition of first row. As shown in Figure 1, the next state of cells is determined with two rows above this state. For reversibility of automata, the row at time (t-2) can be placed after row at time (t-1) and the rules of the reversible automata are applied according to Table 3. The reversible operation is applied and then the initial states is obtained. In Figure 1, the reversible steps are shown in gray color.

**Figure 1.** Performance of Reversible CA.

4. Proposed Method

The proposed method for image cryptography is based on reversible CA. In this method, two one- dimensional reversible CA and one elementary CA are used. The cryptography algorithm is described below:

Step 1: Two rows of input image are read and m (determined by user) number of pixels are selected from two rows. (In Table 2 m is set 2).

Step 2: These pixels in each row are placed in binary way according to its values.

Step 3: According to K that was determined by user binary string in step 2 is divided into k parts. (In table 2 with k=2 the string is divided in 2 parts.)

Step 4: Two produced binary strings are considered as input of reversible CA, and cryptography of numbers is performed by the CA. The output of this step consists of numbers in two times of t and (t-1).

Step 5: In step 4 substituted procedure is performed. Then, in this step the scrambling procedure is applied on the output of previous step by elementary CA for random value generation. Binary strings are connected to each other as output.

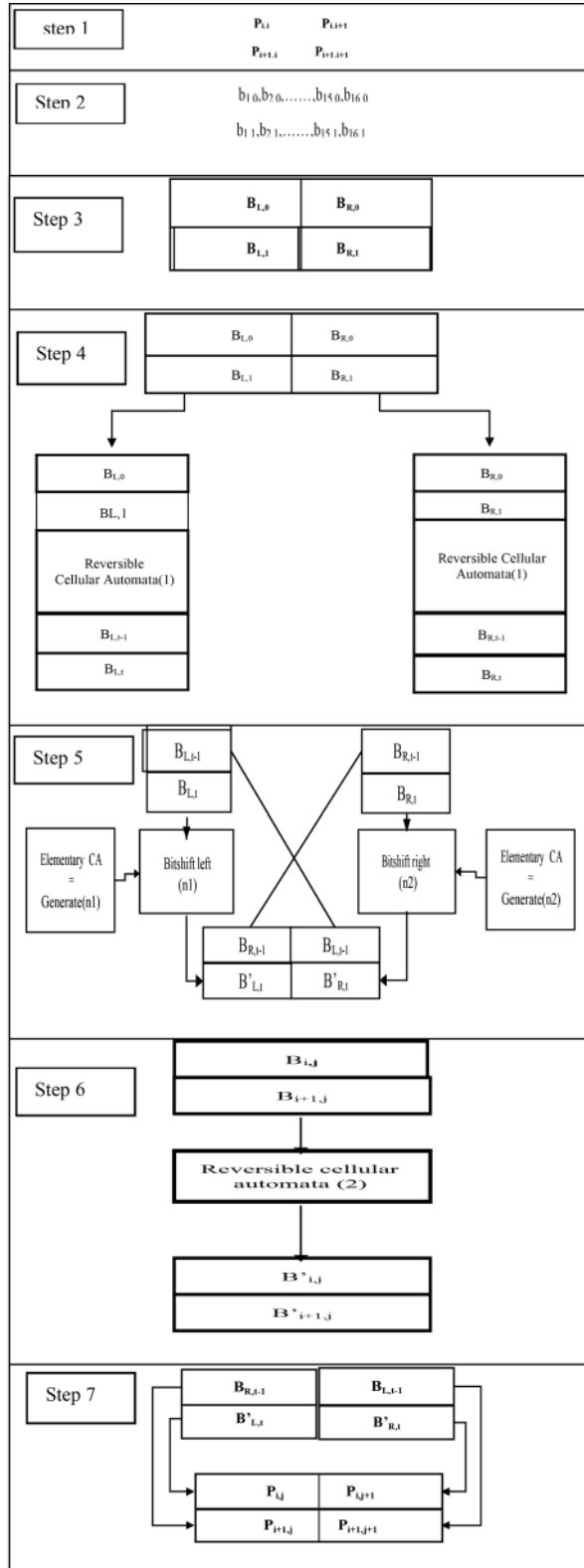
Step 6: Generated data in step 5 feeds as input of another reversible CA and encryption is done.

Step 7: In last step, two outputs are generated for two times of (t) and (t-1), which are the encrypted values of pixels. These values are stored in the encrypted matrix, as shown in Table 4.

In the decryption step, the above steps are applied reversely. Using the encrypted image and the key given as

encrypted matrix in time (t-1), the image can be decrypted reversely according to the algorithm. One example of an iteration of 7 steps is shown in Table 4.

Table 4. Proposed Method



5. Evaluation Result

The results of implementation on cameraman and boats images at sizes of 256×256 with different keys are shown. Figure 2 to 4 illustrate the original, encrypted and decrypted image of cameraman with rules 30, 98, and 153, respectively.

To illustrate the sensitivity of the algorithm to keys in Figure 5, we tried to decrypt the encrypted image with rule 98 with another key. As it is seen, decryption was not done correctly and the image

is completely inaccurate. In Figure 6 to 8, this algorithm has been applied to the image of boats and the results are shown.

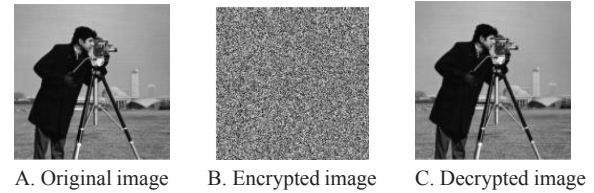


Figure 2. Output Results of Proposed Algorithm With Rule 30

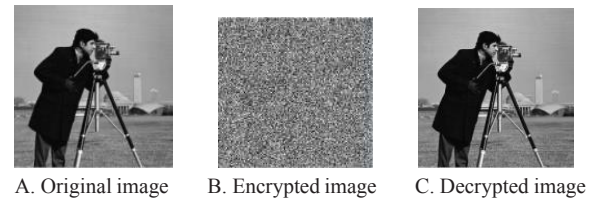


Figure 3. Output Results of Proposed Algorithm With Rule 98

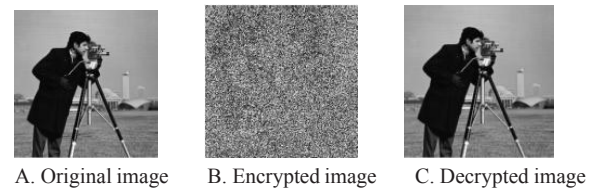


Figure 4. Output results of proposed algorithm with rule 153

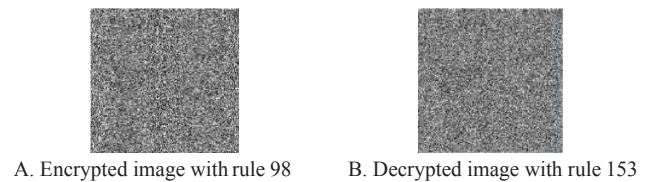


Figure 5. Output results of proposed algorithm with rule 98

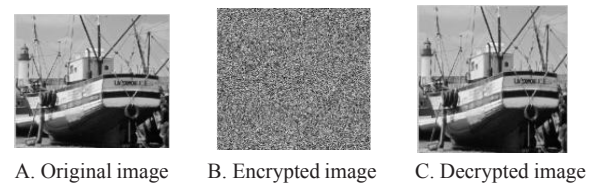


Figure 6. Output results of proposed algorithm with rule 3

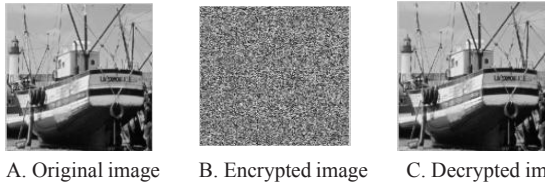


Figure 7. Output results of proposed algorithm with rule 98

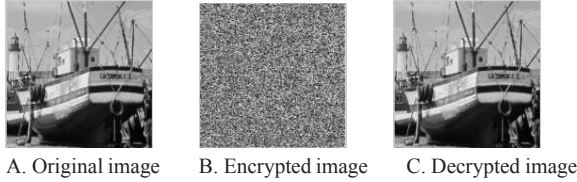


Figure 8. Output results of proposed algorithm with rule 153

6. Analysis and Evaluation of Proposed Method

In this paper, we examined the proposed scheme with [20-23]. In the following, you will see the evaluation of our method in comparison with those methods.

6.1 Statistical Analysis

According to Shannon's theory, attackers can decrypt encrypted image by using statistical analysis. The cryptography algorithm should be such that it will increase the difficulty of statistical analysis. Histogram analysis and correlation coefficients are used to evaluate statistical analysis [22].

6.1.1 Histogram Analysis

A cryptography algorithm is suitable when the image is encrypted in a way that no information is seen from the original image. In other words, the image must not be visually recognizable in cryptography. As the result of the visual test varies from one viewer to another, a histogram analysis can be used. Histogram analysis describes the distribution of the pixels in the image by plotting the number of observations at brightness intensity.

Histogram of original and encrypted images of two cameraman and boats images is shown in Figure 9 and Figure 10, respectively. As seen in the figures, the histogram of the encrypted images is uniform and then it is suitable.

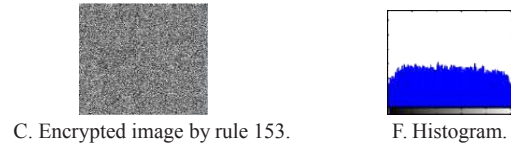
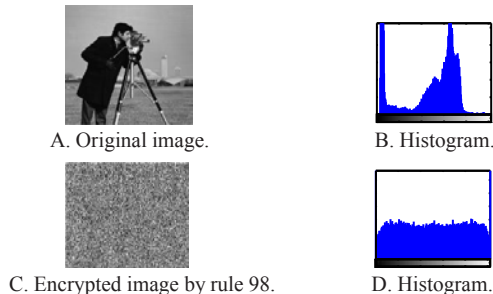


Figure 9. Output Results of Proposed Algorithm with Rule 153

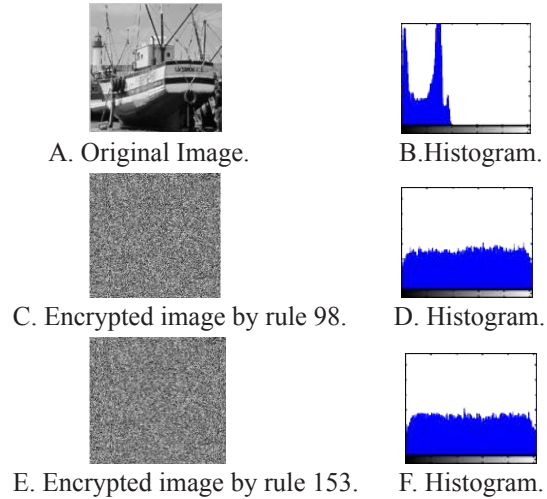


Figure 10. Output Results of Proposed Algorithm With Rule 153.

6.1.2 Correlation Coefficients Analysis

Another evaluation criterion for statistical analysis is correlation. As the correlation of adjacent pixels in the encrypted image is less, the performance of the algorithm would be more suitable [22]. To evaluate the correlation of pixels in horizontal, vertical and diagonal direction, we use Eq. 1. In these equations, x and y are brightness of two adjacent pixels in image and N is the number of pixels selected from image. The values of the correlation in three vertical, horizontal and diagonal directions for the cameraman image and its encrypted images with rules 98 and 153 with four algorithms introduced by [20-23] and the proposed algorithm are shown in Tables 5 and 6, respectively. Based on values, as expected, the pixel correlation of the original image is high. In the encrypted images, this value is reduced and the pixels are less dependent on each other. In the proposed method, this value is less than the other methods, indicating that the proposed method has better performance than others.

$$r_{xy} = \frac{\text{cov}(x, y)}{\sqrt{D(x)}\sqrt{D(y)}} \quad (1)$$

$$\text{cov}(x, y) = \frac{1}{N} \sum_{j=1}^N (x_j - E(x))(y_j - E(y)) \quad (2)$$

$$E(x) = \frac{1}{N} \sum_{j=1}^N x_j \quad (3)$$

$$D(x) = \frac{1}{N} \sum_{j=1}^N (x_j - E(x))^2 \quad (4)$$

Table 5. Values of the Correlation of Cameraman with Rule 98

Correlation	diagonal	vertical	horizontal
Original image	0.9373	0.9546	0.9562
[20]	0.0114	-0.0383	-0.0369
[21]	-0.0178	0.0149	0.0122
[22]	0.0068	-0.0176	-0.0116
[23]	0.0113	0.0337	-0.204
Proposed method	-0.000067	-0.0015	0.0012

Table 6. Values of the Correlation of Cameraman with Rule 153

Correlation	diagonal	vertical	horizontal
Original image	0.9212	0.9536	0.9489
[20]	0.0410	-0.0641	-0.0632
[21]	0.0432	-0.0635	-0.0604
[22]	0.0017	-0.0227	-0.0219
[23]	0.1368	0.2562	0.1541
Proposed method	-0.0015	-0.0052	-0.0166

6.2 Sensitivity Analysis

An ideal property for an encrypted algorithm is sensitivity to small changes in the original image and keys. Three criteria of UACI, MAE, and NPCR are used to test the effect of changing an input pixel on the encrypted image. As these three criteria are higher, the cryptography algorithm would have more efficiency (Kanso and Ghebleh 2012).

Eq. 5 introduced mean absolute error (Jolfaei and Mirghadri 2010). In this equation, $C(i, j)$ and $P(i, j)$ are the pixel values of the encrypted image and the original image, respectively.

Eq. 6 shows the calculation of NPCR, which measures the percentage of different pixels between two cipher images whose plane images have only one pixel difference. $C1$ and $C2$ are two different cipher images whose corre-

sponding plaintext images differ by only one bit [8,20].

The UACI is illustrated in Eq. 8. It measures the average intensity of differences between two cipher images.

Table 7 shows the values of the evaluation criteria for the algorithms introduced by [20-23] and proposed algorithm with rule 153. From table, we can see that the values for the proposed method have the highest value compared to others; that is, the tiny change of pixel in the original image causes great change in encrypted image.

$$MAE = \frac{1}{M \times N} \sum_{i=1}^N \sum_{j=1}^N |C(i, j) - P(i, j)| \quad (5)$$

$$NPCR = \frac{\sum_{i=1}^N \sum_{j=1}^N D(i, j)}{M \times N} \quad (6)$$

$$D(i, j) = \begin{cases} 0 & \text{if } C_1(i, j) \equiv C_2(i, j) \\ 1 & \text{if } C_1(i, j) \neq C_2(i, j) \end{cases} \quad (7)$$

$$UACI = \frac{1}{M \times N} \frac{\sum_{i=1}^N \sum_{j=1}^N C_1(i, j) - C_2(i, j)}{255} \quad (8)$$

Table 7. Values of the MAE, NPCR and UACI

Ref.	MAE	NPCR	UACI
[20]	39.572	49.3057	15.0151
[21]	38.6359	49.4232	13.8246
[22]	74.4251	49.2706	9.6542
[23]	40.8497	50.0253	15.0241
Proposed method	44.7147	50.2045	17.3348

6.3 Entropy Analysis

Entropy is another important characteristics of the randomness of the algorithm. Entropy is calculated according to Eq. 9, where $P(m_i)$ is the number of occurrences of m_i . In an ideal state, for an encrypted image, which each pixel of it is 8 bits, this value should be about 8 [22]. Table 8 shows entropy values for mentioned methods.

$$H(m) = - \sum_{i=0}^{2^N-1} P(m_i) \times \log_2 \left[\frac{1}{P(m_i)} \right] \quad (9)$$

Table 8. Values of Entropy

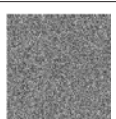
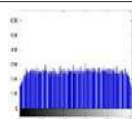
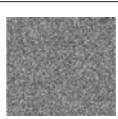
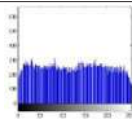

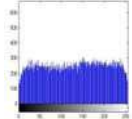
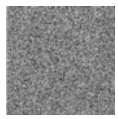
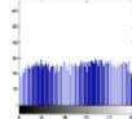
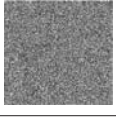
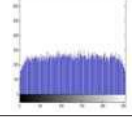
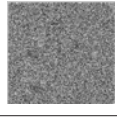
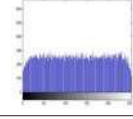
Methods	Proposed method	[20]	[21]	[22]	[23]
Entropy	7.9892	7.9322	7.4259	7.2992	7.9253

6.4 Key Sensitivity Analysis

Key sensitivity is one of the essential characteristics for a cryptography algorithm. This means that changing a bit in the private key should produce a completely different encrypted image. The high sensitivity to the key guarantees the security of the cryptography system against Brute-force attack. To evaluate the characteristics of sensitivity to the key, the original image is encrypted with the one secret key, then, the key is slightly changed and the original image is re-encrypted. If the comparison of these two encrypted images is not possible visually, the encryption algorithm would have high sensitivity to the key.

Table 9 shows the result of the sensitivity to key test. In order to detect the difference of encrypted images, histogram of the images has been plotted to make their comparison easier.

Table 9. Key Sensitivity Analysis

Original key		Slightly changed keys	
Encrypted image	Histogram	Encrypted image	Histogram
			
			
			

6.5 Key Space Analysis

In order to prevent brute-force attack, the key space of the cryptography algorithm should be large enough. The key space of the algorithm contains the total number of available keys in the cryptography algorithm. As the key space of cryptography is larger, the time to test all keys would increase, so it would be resistant to brute-force attack. In the proposed algorithm, four automata are used. Due to the fact that in each automaton, 2^8 rules can be used, the key space is $2^8 \times 2^8 \times 2^8 \times 2^8 = 2^{32} = 4294967296$, so proposed structure is immune to brute-force attack.

6.6 Implementation Analysis

The performance of a cryptography system is evaluated based on various factors such as reliability against various attacks, computational complexity and cryptography time.

In the previous sections, it was observed that the proposed algorithm had a good performance against various attacks. In this section, computational complexity and algorithm implementation time are discussed. The proposed algorithm is performed in three steps and includes various operations, including production of random numbers, linear calculations of CA, shifting, and bit XOR. All of these operations have direct implementation. Therefore, the proposed algorithm is efficient computationally.

7. Conclusion

CA is a useful tool for cryptography. Due to the randomness of the CA, the image can be encrypted with high quality. The reversible CA also has the capability to introduce reversible cryptography techniques on the image. The proposed method uses reversible CA to encrypt the image. In this article, a new structure for image cryptography is introduced, which encrypts the image in three steps. The results of the application of this algorithm on the image compared with the methods introduced in [20-23] by evaluation criteria such as UACI, MAE, and NPCR. The results show that this method has better performance.

References

- [1] A. Jolfaei and A. Mirghadri. A novel chaotic image encryption scheme using chaotic maps. *ADST Journal*, 2011 2: 111-124.
- [2] T. Kumar, S. Chauhan. Image cryptography with matrix array symmetric key using chaos based approach. *International Journal of Computer Network and Information Security*, 2018, 11: 60.
- [3] D. Mewada, N. Dave, and R.K. Prajapati. A Survey: Prospects of Internet of Things Using Cryptography Based on its Subsequent Challenges. *Australian Journal of Wireless Technologies, Mobility and Security*, 2019, 1: 28-30.
- [4] S.S. Moafimadani, Y. Chen, and C. Tang. A New Algorithm for Medical Color Images Encryption Using Chaotic Systems. *Entropy*, 2019, 21: 577.
- [5] H. Gao, Y. Zhang, S. Liang, and D. Li. A new chaotic algorithm for image encryption. *Chaos, Solitons & Fractals*, 2006, 29(2): 393-399.
- [6] X. Xian, J. Liu. Application of Chaos Theory in Incomplete Randomized Financial Analysis, 2019, 2: 3-5.
- [7] A. Ding, W.Q. Yan, and D.X. Qi. Digital image scrambling technology based on Arnold transformation. *Journal of Computer-aided design & Computer Graphics*, 2001, 4: 338-341.
- [8] Y. Luo, J. Yu, W. Lai, and L. Liu, A novel chaotic image encryption algorithm based on improved baker

- map and logistic map, *Multimedia Tools and Applications*, 2019.
- [9] Z.H. Guan, F. Huang, and W. Guan. Chaos-based image encryption algorithm. *Physics Letters A*, 2005, 346: 153-157.
- [10] D.A. Guardeno. Framework for the Analysis and Design of Encryption Strategies Based on Discrete-Time Chaotic Dynamical Systems. Doctoral Thesis, Universidad Politecnica De Madrid, 2009.
- [11] J. Von Neumann. Theory of self-reproducing automata, University of Illinois Press, 1966.
- [12] J. Jin, Z.H. Wu. A secret image sharing based on neighborhood configurations of 2-D cellular automata. *Optics & Laser Technology*, 2012, 44(3): 538-548.
- [13] M. Ahangaran, N. Taghizadeh, and H. Beigy. Associative cellular learning automata and its applications. *Applied Soft Computing*, 2017, 53: 1-18.
- [14] Z. Eslami, S. Razzagh, and J. Zarepour Ahmadabadi. Secret image sharing based on cellular automata and steganography. *Pattern Recognition*, 2010, 43: 397-404.
- [15] P.L. Rosin. Image processing using 3-state cellular automata. *Computer Vision and Image understanding*, 2010, 114: 790-802.
- [16] C. Kauffmann, N. Piché, Seeded ND medical image segmentation by cellular automaton on GPU. *International Journal of Computer Assisted Radiology and Surgery*, 2010, 5: 251-262.
- [17] Z. Eslami, J. Zarepour Ahmadabadi. A verifiable multi-secret sharing scheme based on cellular automata. *Information Sciences*, 2010, 180(1): 2889-2894.
- [18] Y. Ruisong, L. Huiliang. A novel image scrambling and watermarking scheme based on cellular automata. *International Symposium on Electronic Commerce and Security*, 2008: 938-941.
- [19] F. Qadir, M. Peer, and K. Khan. Digital image scrambling based on two dimensional cellular automata. *International Journal of Computer Network & Information Security*, 2013, 5(2): 36-41.
- [20] J. Jin, An image encryption based on elementary cellular automata. *Optics and Lasers in Engineering*, 2012, 50(12): 18396-1843.
- [21] A. Abdo, S. Lian, L. Ismail, M. Amin, and H. Diab. A cryptosystem based on elementary cellular automata. *Communications in Nonlinear Science and Numerical Simulation*, 2013, 18(1): 136-147.
- [22] X. Wang, D. Luan. A novel image encryption algorithm using chaos and reversible cellular automata. *Communications in Nonlinear Science and Numerical Simulation*, 2013, 18(11): 3075-3085.
- [23] F.K. Mohamed. A parallel block-based encryption schema for digital images using reversible cellular automata. *an International Journal of Science and Technology*, 2014, 17: 85-94.
- [24] S. Wolfram. Theory and Application of Cellular Automata. Singapore: World scientific Publishing, 1986.
- [25] M. Esnaashari, M. Meybodi. A novel clustering algorithm for wireless sensor networks using irregular cellular learning automata. in *International Symposium on Telecommunications*, 2008, 330-336.
- [26] S. Roy. A study on delay-sensitive cellular automata. *Physical A: Statistical Mechanics and its Applications*, 2019, 515: 600-616.
- [27] M. Medenjak, V. Popkov, T. Prosen, E. Ragoucy, and M. Vanicat. Two-species hardcore reversible cellular automaton: matrix ansatz for dynamics and no equilibrium stationary state. *arXiv preprint arXiv: 2019: 1903.10590*.
- [28] S. Yingri, Y. Wo, and G. Han. Reversible cellular automata image encryption for similarity search. *Signal Processing: Image Communication*, 2019, 72: 134-147.

ARTICLE

Computation Offloading and Scheduling in Edge-Fog Cloud Computing

Dadmehr Rahbari* **Mohsen Nickray**

Department of Computer Engineering and Information Technology, University of Qom, Qom, Iran

ARTICLE INFO

Article history

Received: 16 August 2019

Accepted: 27 September 2019

Published Online: 18 October 2019

Keywords:

Cloud computing

Edge computing

Fog computing

Offloading

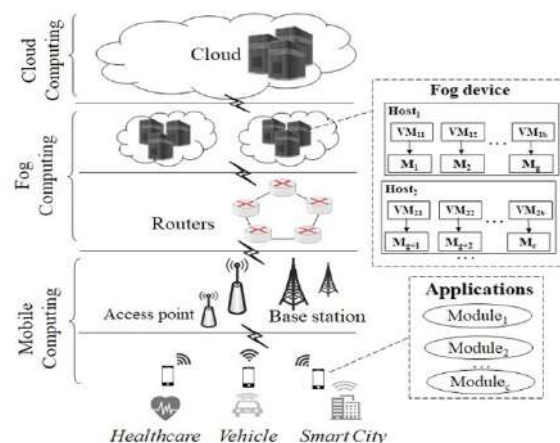
Scheduling

ABSTRACT

Resource allocation and task scheduling in the Cloud environment faces many challenges, such as time delay, energy consumption, and security. Also, executing computation tasks of mobile applications on mobile devices (MDs) requires a lot of resources, so they can offload to the Cloud. But Cloud is far from MDs and has challenges as high delay and power consumption. Edge computing with processing near the Internet of Things (IoT) devices have been able to reduce the delay to some extent, but the problem is distancing itself from the Cloud. The fog computing (FC), with the placement of sensors and Cloud, increase the speed and reduce the energy consumption. Thus, FC is suitable for IoT applications. In this article, we review the resource allocation and task scheduling methods in Cloud, Edge and Fog environments, such as traditional, heuristic, and meta-heuristics. We also categorize the researches related to task offloading in Mobile Cloud Computing (MCC), Mobile Edge Computing (MEC), and Mobile Fog Computing (MFC). Our categorization criteria include the issue, proposed strategy, objectives, framework, and test environment.

1. Introduction

In recent years, wireless sensor networks (WSNs) have been extensively developed independently or partially from another system. WSNs collect data in health-care, vehicles, smart home, and more. These networks as the infrastructure for the IoT require real-time processing and decision-making. Data transmission from end-sensor nodes to the cloud by passing several mid-sensor nodes, routers, and gateways have high total network power consumption and delay^[1]. In many sensitive cases such as medical care and transportation systems, high delays in IoT applications can lead to a patient's death or cause an accident. Edge computing with processing near the IoT devices have been able to reduce the network congestion and delay to some extent, but the problem is distancing itself from

 the Cloud^[2,3].

Figure 1. Architecture of Edge-Fog Cloud computing

*Corresponding Author:

Dadmehr Rahbari,

Department of Computer Engineering and Information Technology, University of Qom, Qom, Iran;

Email: d.rahbari@stu.qom.ac.ir

As a relatively new architecture, FC sits between the cloud and the sensors, so data aggregation, processing, and storage can be done near the sensors, as well as data sent to the cloud data center only if necessary^[4]. Processing operations are performed by the fog nodes at the edge of the network, where the sensors are, so the network traffic decreases and the transport speed increases. Since cloud computing reduces data transfer to the cloud, it consumes less energy than the cloud^[5,6].

According to Figure 1, FC has a hierarchical structure. The sensors are at the lowest level of this architecture, collecting data at specified intervals and delivering it to the fog layer at the mid-level^[7,8]. Fog nodes are responsible for measuring, processing, and sending data to the cloud. At the highest level, the cloud performs heavy storage and processing operations.

Applications in this network can be run by multiple modules by processors. Modules in each FD have different tasks depending on the application type^[9]. As a small data center, FDs implement modules with their resources. An appropriate way of allocating CPUs to modules is to increase the resource efficiency of the fog nodes^[10]. At FC, scheduling resources and modules is a challenge. Resource allocation can be performed according to a number of QoS parameters^[11]. The performance of scheduling algorithms is evaluated using several parameters, such as power consumption, waiting time, execution time, task completion time as well as some security criteria^[12,13].

FC is a great architecture for IoT applications such as smart home, wearables, health care and vehicles^[14, 15]. For example, in a treatment clinic, one or more FDs may be used to monitor the activity of the elderly or special patients. In transportation systems, FD is also used to track and control cars. FC has distributed architecture and cloud has centralized architecture. The main advantage of FC is that it can deliver services provided in cloud data centers on the edge of the network near the end sensors^[6].

Scheduling issues are classified into several types, including resource allocation, load balancing, and offloading. These categories are implemented in various architectures such as cloud, edge, and fog. Scheduling can be monitored using a variety of parameters. There are also different ways to solve these problems, each with its own advantages and disadvantages. This research examines, classifies and analyzes these challenges in various applications including the well-known IoT framework. In fact, this paper categorizes the different methods of computation offloading and scheduling in Cloud, Edge, FC. Also, another classification is presented for offloading mobile computing. The main objectives of this paper are to:

(1) Provide a comprehensive review of the literature in the scheduling and offloading issues.

(2) Categorize scheduling algorithms in a variety of centralized and distributed computing.

(3) We summarize the research findings, conclude the paper, and suggest some research subjects in scheduling scope.

The rest of this article is organized in the following sections. In Section 2, the past works of scheduling methods are provided. The mobile computing is explained in Section 3 and its offloading methods in MCC, MEC, and MFC are presented in Section 4. Section 5 include an analysis and comparison of offloading and scheduling methods. Section 6 presents the summary and conclusions of this work.

2. Scheduling

Scheduling is in many areas. One of the meanings is to plan entry and exit. These include the arrival and departure schedules of ships on the docks^[16-20], trucks in transit^[21-23], industrial equipment^[24], and supply chains^[25]. The second meaning that is most often considered in networks is the allocation of resources to input tasks. Here the second meaning is of interest. Topics such as load balancing, load prediction, reliability and fault tolerance in offloading, resource provisioning, software-defined networking, network function virtualization, and scheduling with fog architecture are considered to be very appropriate developments that are at the beginning of the road today and have a great deal of research.

Scheduling is responsible for optimizing CPU usage and allocating resources appropriately to applications. A scheduler, considering the possible sets of executable tasks, decides in which order and where they will be executed. Scheduling goals include cost, interest, maximization of the number of executable tasks, use of VM or their migration, energy consumption, error tolerance, reliability and security^[26]. Optimization strategies include heuristic^[27], meta-heuristic^[28,29] and other methods. Resource models include different VM deployment patterns, single or multiple providers, medium data-sharing model, data transfer, cost, static and dynamic types, resource sharing, single VM pricing model and Delay is the supply of VM^[28,30].

2.1 Concepts of Resource Management

Customers can request multiple services at the same time. There are various algorithms for allocating resources to input tasks^[13,4]. Resource management has three main functions: provisioning, scheduling, and monitoring^[31].

Resources provisioning: The term resource provision-

ing was used in the grid computing framework. Providing suitable resources to works depends on the QoS parameters. The consumer of the service communicates with the agent of providing resources RPA and sends the application (workflow). The RPA finds the right resources and selects the best one based on customer needs. After submitting the workflow to the RPA Information Center section, access operations are performed according to customer request. The process of selecting the source is the best source for the workflow according to the requirements of the QoS^[31].

Resource Scheduling: Challenges in providing resources include dispersion, uncertainty, and heterogeneity. Resource scheduling includes two functions as the allocation of resources and maps them. The purpose of resource allocation is to allocate appropriate resources for tasks in the correct order so that tasks can use resources effectively. Resource mapping is the process of mapping tasks to suitable resources based on the quality of service and determined by the user in accordance with the SLA agreement. Task scheduling is the allocation of VMs to tasks^[31], that is shown in Figure 2. In this figure, the meaning of the physical machine in the cloud is the host of data center, on the edge means the edge device and, in the fog, the fog device.

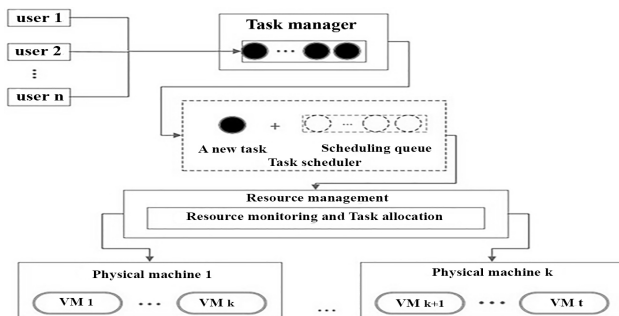


Figure 2. Resource Scheduling

Resource monitoring: Monitoring and controlling resource efficiency can improve system performance. Therefore, a global supervisor is needed to examine how resources are allocated. Supervisory criteria include CPU usage, memory and storage space. The supervisor expects tasks to be executed with minimal cost and time without SLA violation^[31].

2.2 Scheduling Objectives

The scheduling process assigns tasks within workflows to appropriate resources according to specific scheduling criteria. Scheduling parameters are effective in the success of the workflow scheduling problem. Scheduling objectives are classified into two groups based on the service approach: service provider and consumer services^[32].

Consumer Service:

(1) **Makespan:** This criterion is equal to the time all tasks are completed. The makespan can be considered as the length of time the user sends the job until it completes the work and is the results generated.

(2) **Budget:** This is equal to the financial constraint on the use of resources. To run the total workflow can be used several VM from different types. The total cost of execution is equal to the sum of all types of VMs used in the implementation, which should be less than the user-defined budget.

(3) **Deadline:** Critical applications need to be completed within a certain time period. Scheduling is defined under the time limitation for the applications to be completed before the deadline.

(4) **Security:** In distributed computing such as Fog, resources are varied and vast, so maintaining security is an important issue. Data protection and privacy in the haze environment are more complex than traditional systems because of the nature of the distribution.

(5) **Cost:** This parameter includes computing costs, data transmission costs, and storage costs^[32].

Service Provider:

(1) **Load balancing:** VMs are the most important resource in the computing environment. On scheduling, you can assign more than one task to a VM to run tasks simultaneously, which results in load imbalances on VMs. Load balancing between resources improves resource efficiency and thus improves the overall performance of the scheduling process.

(2) **Consuming resources:** Increasing the use of resources for a helpful service provider.

To obtain the maximum benefit is allocated limited resources to the user, are fully used resources.

(3) **Energy efficiency:** The use of processors and the use of resources directly affects the energy consumed by a task. When the processor is not used properly, the energy consumption will be high because is not effectively used the idle time^[32].

2.3 Traditional Methods

The authors in^[33] devised a dynamic programming (DP) method for allocating resources to runtime constrained input tasks. In this way, each provider offers several different VMs and global services for data sharing. One of the methods of resource allocation is the fastest time-out algorithm that has increased cost. In^[34], researchers analyzed the Multi-Objective Optimization (MOO) method for business infrastructure services. They used the Pareto Front as a de-

cision-making method for trading optimal solutions. They cut the cost of the timetable by half, but increased the rate by 5%. In another paper, resource allocation is performed considering the fault tolerance according to the proposed method for point-and-time VMs for executing user requests. Prices have started roughly and increased during execution to get closer to user demand. The results show that due to the use of spot VM^[35] the scheduling performance is low. n^[36], a method of allocating resources based on hardware defects in instant time is presented. This method has three steps in term of elastic resource provisioning in the clouds. First, backward shifting of overlapping tasks with VM migration. Second, increasing the resource scale to increase the capability of VM operations or builds due to synchronization with subsequent input work. Third, shrinking of the processing capacity of an idle VM. The results of this work caused to optimized resource utilization than other baseline algorithms.

In^[37], the authors investigated QoS parameters using three resource allocation algorithms in the Fog architecture, namely: concurrent priority, first-input-first-output, and delay priority. In the concurrent method, input tasks are assigned to them regardless of the capacity of the resources. In the first-input-first-output method, tasks are executed the same way they were entered. If the data center is unable to execute the request, then the task is queued. In priority delay-based methods, the input tasks are executed based on the least time delay. The paper uses the iFogsim simulator^[1] with two applications of brain signal tracking and object tracking in video images. The results show that the concurrent method has more delay than the first-input-first-output and delay priority method. In tracking brain signals, the number of modules per device for the simultaneous method is greater than the other two. The number of modules in the cloud for the first-in-first-out method was higher than the other two.

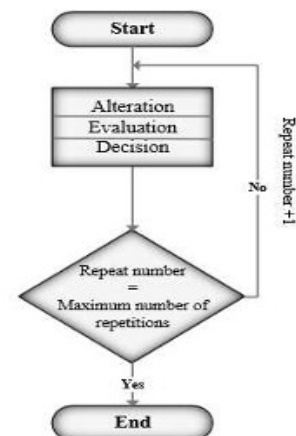
2.4 Heuristic Methods

In heuristic algorithms, the answers are obtained by a number of rules. In the classical type of these algorithms, there are methods such as first, best and worst fit. Major resource allocation^[28] issues in Fog can be solved by such methods. In^[38], the input tasks are programmed by a heuristic algorithm, which aims to reduce the cost of executing the tasks. Performance and cost improved, according to the results. In^[39], parallel tasks were implemented by instantaneous execution on a network of different sources by a heuristic. Researchers selected the frequency of sources using nonlinear programming (NLP).

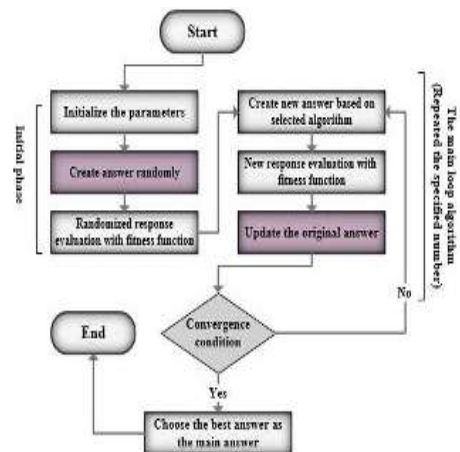
In^[40], a knapsack-based scheduler for parallel transmission of video content is presented. The researchers imple-

mented the max-min method on high-powered computers for mapping tasks in a number of sectors. The analysis of the results proves that their proposed method has improved at runtime and number of segments. Researchers in^[41] solved the task scheduling problem in fog-based IoT applications by knapsack. They optimized knapsack by symbiotic organism search. The results revealed superiority than other methods. In another study^[42], a backpack algorithm with dynamic programming was used to solve the resource allocation problem with the aim of reducing runtime and cost. Their major achievements have been the use of low-capacity resources and effective quantities for time-lapse parameters, network congestion, and precise job size.

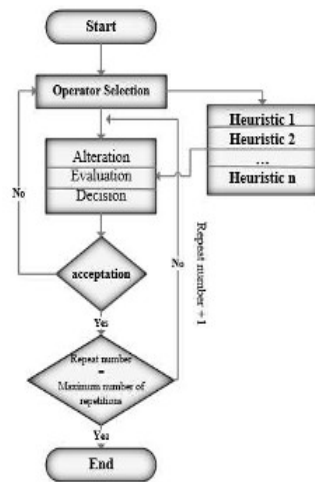
The general process of heuristic algorithms is shown in Figure 3a. The flowchart of population-based algorithms is similar to Figure 3b, with the difference that instead of a solution, is created a set of solution. Hyper-heuristic algorithms (Figure 3c) are the exploratory search method in which automation, often combined with the techniques of machine learning, is the process of selecting, combining, producing or modifying several simple heuristics for solving computational problems.



(a) Heuristic Algorithm -



(b) Meta-Heuristic Algorithm



(c) Hyper-Heuristic Algorithm

Figure 3. Flowchart of approximate algorithms

2.5 Meta-heuristic Methods

One of the extra-heuristic algorithms to solve the resource allocation problem is the PSO optimization method presented in [11]. One of the features of this method is the provision of elastic and different sources with infinite resources as well as changing VM operation. One of the problems with this approach is the computational overhead for resource providers, which increased by the number of VMs and tasks [11]. A hybrid algorithm involving PSO and cats' optimization for resource allocation and VM management in the cloud has reduced the average response time, also it has increased resource utilization by up to 12% in compared with other benchmark algorithms [43]. ACO-based scheduling ACO has been used as another evolutionary algorithm for scheduling and resource allocation in the cloud, which has been more effective in the loading of resources and reducing of request failures. It used the fitness function based on trusted values and deadlines. As results, ACO minimized the throughput and the number of request failure and maximized the computation power [10]. The different scheduling problem solved in [44] by knapsack and optimized by ant colony optimization (ACO). In [45], resource allocation in the cloud is solved by the KnapGA genetic backpack algorithm. Its graceful function includes CPU utilization, network power, disk input, and output times. The researchers were able to reduce the energy consumption and migration of VMs.

Another meta-heuristic approach presented in [46] is the Bee-Based Algorithm for allocating resources to tasks in the fog network. Their algorithm as BLA is based on the optimized distribution of tasks in the fog nodes. The researchers using BLA find an optimal tradeoff between runtime and memory allocation for mobile users. The results show that runtime and memory allocation values by

BLA are lower than GA and PSO algorithms.

The authors in [47] studied the resource allocation based on the meta-heuristic methods in the clouds. Each algorithm has some advantages and disadvantages. Scheduling solutions have issues like resource scaling, failure handling, security and storage-aware, dependent tasks, data transfer cost, dynamic resource provisioning for the IoT. In [48], resources are allocated to tasks in FC by NSGA-II method. This work simulated in MATLAB. They only compare their method with random allocation method. Their scheduling method reduced the latency and improve the stability of the task execution.

Studies show that much has been done in the field of cloud computing in the Cloudsim simulator [49]. Of course, a number of FC-related work has been done on Cloudsim or different programming frameworks. iFogsim, as successful development of Cloudsim, is very applicable to FC scheduling and resource management algorithms. The analysis of the heuristic algorithms proves that these methods have a long runtime and are not suitable for delay-sensitive scheduling problems.

We compare the mentioned scheduling methods by the problem, algorithm, objectives, framework, and environment in Table 1. The problems are categorized by task/job scheduling and resource provisioning.

Table 1. Summary of scheduling algorithms

Algorithm	Problem	Objectives	Framework	Environment
Knapsack [40]	Task scheduling	Complete time	Cloud	Matlab
Knapsack [42]	Task scheduling	Deadline and cost	Cloud	Cloudsim
KnapGA [45]	Task scheduling	I/O rate, migration count, and host occupation	Cloud	Simulation
ACO [10]	Task scheduling	Trust value and deadline	Cloud	Simulation
PSO [11]	Resource provisioning	Deadline and cost	Cloud	Simulation
DP [33]	Task scheduling	Deadline and cost	Cloud	Fabric compiler
MOO [34]	Task scheduling	Earliest finish time and completion time	Cloud	Real
Bidding strategy [35]	Task scheduling	Deadline, cost, and reliability	Cloud	Cloudsim
Backward shifting [36]	Resource provisioning	Host failure and task starting time	Cloud	Cloudsim
PSO [43]	Task Scheduling	Utilization of VMs and Response time	Cloud	Python
ACO [44]	Task scheduling	Start time	Smart Grid	Matlab
Heuristic [38]	Task scheduling	Makespan and execution cost	Cloud-Fog	Cloudsim
NSGA-II [48]	Resource scheduling	latency and stability	Fog	Matlab

Mobility aware ^[37]	Task scheduling	Costs and QoS	Fog	iFogsim
NLP ^[39]	Task scheduling	Energy of thread execution	Fog	Simulation
BLA ^[46]	Job scheduling	Run time and memory allocation	Fog	BLA with C++
HHS ^[26]	Task scheduling	Security, CPU, and bandwidth	Fog	iFogsim
GKS ^[27]	Task scheduling	Cost and Energy	Fog	iFogsim
KnapSOS ^[41]	Task scheduling	CPU and bandwidth	Fog	iFogsim

3. Mobile Computing

The executing computation tasks of mobile applications on MDs requires a lot of resources, so they can offload to the Cloud. But Cloud is far from MDs and has challenges as high delay and power consumption. In general, mobile computing falls into the following three categories.

(1) MCC: Some processes on mobile devices require robust resources so they must be sent to the cloud data center. If a large number of users are logged in with delay-sensitive applications and want to cloud the data, then there is the problem of bandwidth ^[50, 2].

(2) MEC: In this type, tasks are performed near the mobile device ^[51]. Mobile edge computing reduces network congestion and performs tasks more efficiently ^[2].

(3) MFC: Since the cloud is far away from mobile devices ^[52], it is possible to send delay-sensitive tasks to the fog layer. As a result, it will save time and energy ^[53].

MFC can speed up the transfer of tasks to data centers ^[54]. This inexpensive and low-latency network architecture can be used as an infrastructure for the IoT.

4. Offloading

The issue of offloading in mobile computing has become an attractive topic for study and research in recent years. This issue has optimization goals that are outlined below. The objectives of offloading and scheduling in the reviewed articles are as shown in Figure 4.

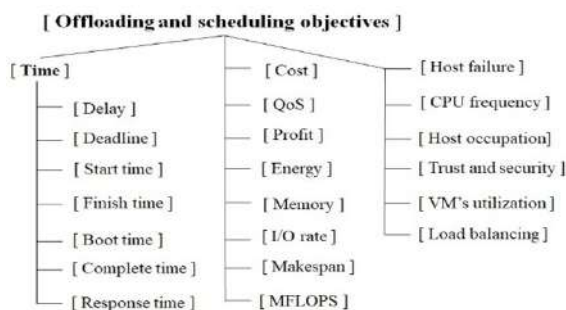


Figure 4. The offloading and scheduling objectives

4.1 MCC-based Offloading

Researchers in ^[55] addressed the problem of offloading and allocation of resources at MCC with the aim of reducing energy consumption. This has limitations such as response time, execution time and cost. The problem-solving method has been a greedy algorithm that has been able to optimize the target criteria. In ^[56], the authors developed an optimal pricing model (OPS) by examining the behavior of mobile users. This has led to a compromise between energy consumption and time delays.

The authors in ^[57] calculated the waiting time of cloud data centers and presented an offloading algorithm as HCOA based on the PSO. In ^[58], the ant colony-based offloading method as CMSACO is presented. The objectives of this method are profit, deadline, task dependency, resource differences, and load balancing. The analysis of results proves that total profits, time spent completing tasks, and network resource consumption have improved.

4.2 MEC-based Offloading

Various algorithms for resource allocation and offloading have been proposed in the MEC ^[59,60]. The authors addressed this in ^[60] and were able to reduce the cost of mobile devices by proving the Nash equilibrium.

In ^[61], the authors propose a functional architecture for different methods of offloading on mobile and IoT devices. In ^[62], the problem of offloading and allocating resources solved by the maximum greedy algorithm called by DGMS. They first introduced the policy of collecting energy for wireless devices from the environment. Then Lyapunov optimization method for loading is presented. The results show the superiority of the proposed method over-centralized and random planning methods.

4.3 MFC-based Offloading (Module Placement)

In ^[63], the problem of offloading mobile device codes in MFC is solved. The researchers compared their approach to VM-based methods and container models. The proposed model performs better than others in the criteria of time delay, memory consumption, and image size and energy consumption. Another method of solving the offloading problem in FC is queue theory ^[53]. The authors proposed a multi-objective optimization method (MOIPM). They were able to improve energy consumption, delay in execution and cost.

In ^[64], the load of informed social calculation is provided for MFC. The proposed method is based on different queue models and energy collection models. Their algorithm has been able to reduce the running cost by solving the Nash generalized equilibrium problem. In ^[65],

researchers provided a task offloading method in MFC by classification and regression tree. They could optimize their method by Markov chain process.

The offloading algorithm presented in [66] is based on machine learning. The proposed method reduces the space of the answers by applying the Markov process and deep reinforcement learning. This method, called DQLCM, has been able to minimize latency.

4.4 MCC/MEC/MFC-based Offloading

Many studies have been presented in integrated architectures [67, 68]. The researchers [68] presented an integrated architecture of the cloud, edge, and IoT that reduced energy consumption. In [69], the offloading and scheduling problem is solved using the complex nonlinear programming method (integer). The researchers were able to reduce the most weight-related to cost, energy consumption and time delay criteria. In [70], the problem of offloading application code in hybrid cloud, edge and fog architecture is provided. The proposed method, SIMD, improves energy consumption, time, and the number of executable instructions as well as the migration overhead.

The mentioned offloading algorithms are summarized in Table 2. The problems are categorized by task and code offloading.

Table 2. Summary of offloading algorithms

Algorithm	Problem	Objectives	Framework	Environment
GABTS [55]	Task offloading and scheduling	Energy, response time, deadline, and cost	MCC	C++
OPS [56]	Task offloading and scheduling	Energy and delay	MCC	ThinkAir
HCOA [57]	Task offloading and scheduling	Energy	MCC	Simulation
CMSACO [58]	Multi-Task offloading	Profit and completion time	MCC	Simulation
W5 [61]	Task offloading	g CPU, memory, and network usage	MEC/MCC	Real
JCORAO [60]	Task offloading and scheduling	Deadline and cost	MEC	Hetnet simulation
DGMS [62]	Multi-Task offloading	Energy, battery, and CPU frequency	MEC	Simulation
Unikernel [63]	Code Offloading	Boot time, memory, and energy	MFC	Android-x86
MOIPM [53]	Task offloading	Energy, delay, and cost	MFC	Simulation
MPMCP [65]	Task offloading	Power, QoS, and security	MFC	Cloudsim

GNP [64]	Task offloading	Cost	MFC	Simulation
DQLCM [66]	Task offloading	Delay and Energy	MFC	Real
MINP [69]	Task offloading and scheduling	Delay, Energy, and Cost	MFC/MCC	Matlab
SIMD [70]	Code Offloading	Energy, execution time, and MFLOPS	FC/MEC/MCC	Real

5. Conclusion and Suggestion

In this paper, we survey recent researches of computation offloading and scheduling in Cloud, edge, and FC. Challenges include time delay, energy, cost, trust, QoS, stability, memory, and security. Our categorizations are based on the issue, proposed strategy, objectives, framework, and test environment of various works. Moreover, based on the analysis, we propose machine learning algorithms to make smart distributed computing environments. We propose the machine learning methods to intelligent task scheduling and offloading in distributed computing. To simulate Cloud and FC applications, the Cloudsim and iFogsim libraries are closer to the real environment.

Studies show that fog computing has been more effective than cloud computing in implementing IoT scheduling and resource management algorithms. Things like power consumption, time delays, and optimizing server shutdown times are much easier in fog computing than cloud computing. Heavy processing is done instead of moving to cloud data centers in fog devices near the end users' location. Based on this study, the following can be suggested for future research:

(1) Applying Machine Learning Techniques: Extensive methods of artificial intelligence and machine learning can be very useful in various applications of IoT. Artificial intelligence methods have shown to be highly effective in a variety of issues. In the scheduling problem, applying these algorithms will help the system learn more and provide better solutions. By focusing on new classifications and adjusting the parameters of these algorithms according to the workflows and resources, it is possible to strive for better performance of the scheduling algorithms.

(2) Applications: One of the case studies could be the definition of new application models in IoT with different computations in fog computing. These include medical care, smart home, smart city, transportation system, car park, instant video analysis, traffic lights management, computer games, big data analytics, energy industry, water, and soil management.

(3) Objective Criteria: Many parameters can be investigated, some of which are: time (start, end, completion,

wait, delay, and deadline), energy consumption, renewable energy, bandwidth, network resource consumption, efficiency, entry rate tasks, accuracy, cost, quality of service, location awareness, mobility, and inter-network connectivity.

(4) Security services: Considering more services in the security overhead model in addition to the three authentication, confidentiality and integration services as well as analyzing these issues in managing and allocating resources to input tasks can be introduced as another area of research.

(5) Scheduling Challenges in the IoT: Research on topics such as load balancing, load prediction, reliability and fault tolerance in offloading, resource provisioning, software-defined networking, network function virtualization and scheduling with fog architecture are considered to be very suitable developments that are at the beginning of the road today and very They have research. The following is a brief explanation of each:

A. Load balancing in fog computing is related to the placement of modules in the appropriate fog device, which requires the development of new methods and models.

B. Forecasting on the IoT can be a very useful topic. Since in dynamic systems, the rate of entry of tasks into the system varies, so it is very difficult to predict. On the other hand, its prediction can be considered as a pre-processing operation in scheduling and resource allocation operations and can improve it. Artificial intelligence methods work very well in this regard. For example, neural network-based approaches such as deep learning and reinforcement can be effective.

C. Trust in fog computing or IoT can be followed by block chain technology because there is no centralized server in distributed systems and so it is very close to the architecture of the hub. On trust, the goal is that new modules, before moving on to the new haze tool, ask their neighbors to trust the haze tool, which can be the subject of much research with mathematical modeling and intelligent algorithms.

D. Fault tolerance is also one of the most commonly used fields in fog computing. There are various methods in this area that examine the error and the solution to reduce or reduce it before and after it occurs.

E. Resource provisioning is one of the special challenges in fog computing that differs with resource allocation. Here are some ways to create or restore resources in the system.

F. Software-defined networks can be explored in fog computing. In this regard, the control section of the network is separated from its forwarding section, and the expressions in the network (such as router and switch) be-

come ineffective decision-making tools and only perform tasks based on the flow tables that the controller communicates to them. Therefore, the programming algorithms of this section are very useful.

G. Network function virtualization is able to implement network elements as software components. Each of these components was traditionally implemented as a separate hardware device. For example, in a network, firewall, router, and load balancing tools have been the norm. Obviously, having separate devices for each application is very costly and has many management complexities. In fog architecture, setting up such sections in virtual terms is very useful and new.

(6) New architectures: Investigating new architectures such as cloud computing increases productivity and reduces time delays in IoT applications and can therefore extend the boundaries of knowledge. These include the dew architecture or network slicing. Given the growing number of network tools, this can be of interest to network architecture professionals.

(7) Development of new software frameworks: Due to the high cost of network tools and the large geographical location needed to test the methods, researchers can develop new simulation environments in fog architecture. Special frameworks can be designed for specific applications that are close to the IoT.

References

- [1] Gupta, H. Vahid Dastjerdi, A. Ghosh, S. K. Buyya, R. ifogsim: A toolkit for modeling and simulation of resource management techniques in the internet of things, edge and fog computing environments, *Software: Practice and Experience*, 2017, 47(9): 1275-1296.
- [2] Gusev, M. Dustdar, S. Going back to the roots-the evolution of edge computing, an iot perspective, *IEEE Internet Computing*, 2018, 22(2): 5-15.
- [3] Dizdarević, J., Carpio, F., Jukan, A., Masip-Bruin, X. A survey of communication protocols for internet of things and related challenges of fog and cloud computing integration. *ACM Computing Surveys (CSUR)*, 2019, 51(6): 116.
- [4] Gill, S. S., Chana, I., Singh, M., Buyya, R. RADAR: Self-configuring and self-healing in resource management for enhancing quality of cloud services. *Concurrency and Computation: Practice and Experience*, 2019, 31(1): e4834.
- [5] Aazam, M. St-Hilaire, M. Lung, C. H. Lambadaris, I. Pre-fog: Iot trace based probabilistic resource estimation at fog, in: *Consumer Communications and Networking Conference (CCNC)*, 2016 13th IEEE

- Annual, Las Vegas, NV, USA, 9-12, IEEE, 2016: 12-17.
- [6] Mahmud, R. Kotagiri, R. Buyya, R. Fog computing: A taxonomy, survey and future directions, in: *Internet of Everything*, Springer, 2018: 103-130.
- [7] Rahmani, A. M. Gia, T. N. Negash, B. Anzanpour, A. Azimi, I. Jiang, M. Liljeberg, P. Exploiting smart e-health gateways at the edge of healthcare internet-of-things: a fog computing approach, *Future Generation Computer Systems*, 2017: 641-658.
- [8] Yousefpour, A., Fung, C., Nguyen, T., Kadiyala, K., Jalali, F., Niakanlahiji, A., Jue, J. P. All one needs to know about fog computing and related edge computing paradigms: A complete survey. *Journal of Systems Architecture*, 2019.
- [9] Satyanarayanan, M. Bah, P. Caceres, R. Davies, N. The case for vm-based cloudlets in mobile computing, *IEEE pervasive Computing*, 2009, 8(4): 14-23.
- [10] Gupta, P. Ghrera, S. P. Trust and deadline aware scheduling algorithm for cloud infrastructure using ant colony optimization, in: *Innovation and Challenges in Cyber Security (ICICCS-INBUSH)*, International Conference on, Noida, India, 3-5. IEEE, 2016: 187-191.
- [11] Rodriguez, M. A. Buyya, R. Deadline based resource provisioning and scheduling algorithm for scientific workflows on clouds, *IEEE Transactions on Cloud Computing*, 2014, 2(2): 222-235.
- [12] Yakubu, J., Christopher, H. A., Chiroma, H., Abdullahi, M. Security challenges in fog-computing environment: a systematic appraisal of current developments. *Journal of Reliable Intelligent Environments*, 2019: 1-25.
- [13] Wang, T., Liang, Y., Jia, W., Arif, M., Liu, A., Xie, M. Coupling resource management based on fog computing in smart city systems. *Journal of Network and Computer Applications*, 2019, 135: 11-19.
- [14] Chen, N. Chen, Y. Smart city surveillance at the network edge in the era of iot: Opportunities and challenges, in *Smart Cities*, , 2018: 153-176.
- [15] Hosseinian-Far, A. Ramachandran, M. Slack, C. L. Emerging trends in cloud computing, big data, fog computing, iot and smart living, in *Technology for Smart Futures*, Springer, 2018: 29-40.
- [16] Umang, N., Bierlaire, M., & Erera, A. L. Real-time management of berth allocation with stochastic arrival and handling times. *Journal of Scheduling*, 2017, 20(1): 67-83.
- [17] Zhen, L., Liang, Z., Zhuge, D., Lee, L. H., & Chew, E. P. Daily berth planning in a tidal port with channel flow control. *Transportation Research Part B: Methodological*, 2017, 106: 193-217.
- [18] Dulebenets, M. A. A comprehensive multi-objective optimization model for the vessel scheduling problem in liner shipping. *International Journal of Production Economics*, 2018, 196: 293-318. .
- [19] Xiang, X., Liu, C., & Miao, L. Reactive strategy for discrete berth allocation and quay crane assignment problems under uncertainty. *Computers & Industrial Engineering*, 2018, 126: 196-216.
- [20] Dulebenets, M.A. A Delayed Start Parallel Evolutionary Algorithm for Just-in-Time Truck Scheduling at a Cross-Docking Facility. *International Journal of Production Economics*. 2019, 212: 236-258.
- [21] Dulebenets, M.A. A Comprehensive Evaluation of Weak and Strong Mutation Mechanisms in Evolutionary Algorithms for Truck Scheduling at Cross-Docking Terminals. *IEEE Access*. 2018, 6: 65635-65650.
- [22] Serrano, C.; Delorme, X.; Dolgui, A. Scheduling of truck arrivals, truck departures and shop-floor operation in a cross-dock platform, based on trucks loading plans. *International Journal of Production Economics*. 2017, 194: 102–112.
- [23] Khalili-Damghani, K.; Tavana, M.; Santos-Arteaga, F.J.; Ghanbarzad-Dashti, M. A. A customized genetic algorithm for solving multi-period cross-dock truck scheduling problems. *Measurement*. 2017, 108: 101–118.
- [24] Ertem, M., Ozcelik, F., & Saraç, T. Single machine scheduling problem with stochastic sequence-dependent setup times. *International Journal of Production Research*, 2019, 1-17.
- [25] Dong, C.; Li, Q.; Shen, B.; Tong, X. Sustainability in Supply Chains with Behavioral Concerns. *Sustainability*, 2019, 11: 4071.
- [26] Rahbari, D., Kabirzadeh, S., and Nickray, M.. A security aware scheduling in fog computing by hyper heuristic algorithm. In *Intelligent Systems and Signal Processing (ICSPIS)*, 2017 3rd Iranian Conference on. IEEE, 87-92.
- [27] Rahbari, D., Nickray, M. Low-latency and energy-efficient scheduling in fog-based IoT applications. *Turkish Journal of Electrical Engineering & Computer Sciences*, 2019, 27(2): 1406-1427.
- [28] Rodriguez, M. A. Buyya, R. A taxonomy and survey on scheduling algorithms for scientific workflows in iaas cloud computing environments, *Concurrency and Computation: Practice and Experience*, 2017, 29 (8): 1-23.
- [29] Raidl, G. R., Puchinger, J., Blum, C. Metaheuristic Hybrids. In *Handbook of Metaheuristics*. Springer, Cham, 2019: 385-417.
- [30] Frincu, M. E. Genaud, S. Gossa, J. Comparing pro-

- visioning and scheduling strategies for workflows on clouds, in: Parallel and Distributed Processing Symposium Workshops and PhD Forum (IPDPSW), 2013 IEEE 27th International, Cambridge, MA, USA, 20-24 May, IEEE, 2013, pp. 2101-2110.
- [31] Singh, S., & Chana, I. A survey on resource scheduling in cloud computing: Issues and challenges. *Journal of grid computing*, 2016, 14(2): 217-264.
- [32] Singh, P., Dutta, M., & Aggarwal, N. A review of task scheduling based on meta-heuristics approach in cloud computing. *Knowledge and Information Systems*, 2017, 52(1): 1-51.
- [33] Malawski, M. Figiela, K. Bubak, M. Deelman, E. Nabrzyski, J. Scheduling multi-level deadline-constrained scientific workflows on clouds based on cost optimization, *Scientific Programming* 2015, 5-5.
- [34] Durillo, J. J., Prodan, R. Multi-objective workflow scheduling in amazon ec2, *Cluster computing*, 2014, 17 (2): 169-189.
- [35] Poola, D., Ramamohanarao, K., Buyya, R. Fault-tolerant workflow scheduling using spot instances on clouds, *Procedia Computer Science*, 2014, 29: 523-533.
- [36] Zhu, X., Wang, J., Guo, H., Zhu, D., Yang, L. T., Liu, L. Fault-tolerant scheduling for real-time scientific workflows with elastic resource provisioning in virtualized clouds, *IEEE Transactions on Parallel and Distributed Systems*, 2016, 27 (12): 3501-3517.
- [37] Bittencourt, L. F., Diaz-Montes, J., Buyya, R., Rana, O. F., Parashar, M. Mobility-aware application scheduling in fog computing, *IEEE Cloud Computing*, 2017, 4(2): 26-35.
- [38] Pham, X. Q., Huh, E. N. Towards task scheduling in a cloud-fog computing system, in: *Network Operations and Management Symposium (APNOMS)*, 2016 18th AsiaPacific, Kanazawa, Japan, 5-7, IEEE, 2016: 1-4.
- [39] Zahaf, H. E., Benyamina, A. E. H., Olejnik, R., Lipari, G. Energy-efficient scheduling for moldable real-time tasks on heterogeneous computing platforms, *Journal of Systems Architecture*, 2017, 74: 46-60.
- [40] Lao, F. Zhang, X. Guo, Z. Parallelizing video transcoding using map-reduce-based cloud computing, in: *Circuits and Systems (ISCAS)*, 2012 IEEE International Symposium on, Seoul, South Korea, 20-23 May, IEEE, 2012: 2905-2908.
- [41] Rahbari, D., Nickray, M. Scheduling of fog networks with optimized knapsack by symbiotic organisms search. In *2017 21st Conference of Open Innovations Association (FRUCT)*. IEEE, 2017: 278-283.
- [42] Rodriguez, M. A. Buyya, R. A responsive knapsack-based algorithm for resource provisioning and scheduling of scientific workflows in clouds, in: *Parallel Processing (ICPP)*, 2015 44th International Conference on, Beijing, China, 1-4, IEEE, 2015: 839-848.
- [43] Guddeti, R.M., Buyya, R., et al. A hybrid bio-inspired algorithm for scheduling and resource management in cloud environment', *IEEE Transactions on Services Computing*, 2017.
- [44] Rahim, S., Khan, S. A., Javaid, N., Shaheen, N., Iqbal, Z., Rehman, G. Towards multiple knapsack problem approach for home energy management in smart grid, in: *Network-Based Information Systems (NBIS)*, 2015 18th International Conference on, Taipei, Taiwan, 2-4, IEEE, 2015: 48-52.
- [45] Chen, S. Wu, J. Lu, Z. A cloud computing resource scheduling policy based on genetic algorithm with multiple fitness, in: *Computer and Information Technology (CIT)*, 2012 IEEE 12th International Conference on, Chengdu, China, 27-29, IEEE, 2012: 177-184.
- [46] Bitam, S. Zeadally, S. Mellouk, A. Fog computing job scheduling optimization based on bee's swarm, *Enterprise Information Systems* 0, 2017: 1-25.
- [47] Sheff, I., Magrino, T., Liu, J., Myers, A. C., van Renesse, R. Safe serializable secure scheduling: Transactions and the trade-off between security and consistency, in: *Proceedings of the 2016 ACM SIGSAC Conference on Computer and Communications Security*, Vienna, Austria, 24-28, ACM, 2016: 229-241.
- [48] Sun, Y. Lin, F. Xu, H. Multi-objective optimization of resource scheduling in fog computing using an improved nsga-ii, *Wireless Personal Communications*, 2018: 1-17.
- [49] Calheiros, R. N., Ranjan, R., Beloglazov, A., De Rose, C. A., Buyya, R. Cloudsim: a toolkit for modeling and simulation of cloud computing environments and evaluation of resource provisioning algorithms, *Software: Practice and experience*, 2011, 41 (1): 23-50.
- [50] Fernando, N. Loke, S. W. Rahayu, W. Mobile cloud computing: A survey, *Future generation computer systems*, , 2013, 29(1): 84-106.
- [51] Mach, P. Becvar, Z. Mobile edge computing: A survey on architecture and computation offloading, *IEEE Communications Surveys & Tutorials*, 2017, 19(3): 1628-1656.
- [52] Li, C., Xue, Y., Wang, J., Zhang, W., Li, T. Edge-oriented computing paradigms: A survey on architecture design and system management, *ACM Computing Surveys (CSUR)*, 2018, 51(2): 39.
- [53] Liu, L., Chang, Z., Guo, X., Mao, S., Ristaniemi, T.

- Multiobjective optimization for computation offloading in fog computing, *IEEE Internet of Things Journal*, 2018, 5(1): 283-294.
- [54] Roman, R., Lopez, J., Mambo, M. Mobile edge computing, fog et al.: A survey and analysis of threats and challenges, *Future Generation Computer Systems*, 2018, 78: 680-698.
- [55] Tang, C., Wei, X., Xiao, S., Chen, W., Fang, W., Zhang, W., Hao, M. A mobile cloud-based scheduling strategy for industrial internet of things, *IEEE Access*, 2018, 6: 7262-7275.
- [56] Shah-Mansouri, H., Wong, V. W., Schober, R. Joint optimal pricing and task scheduling in mobile cloud computing systems, *IEEE Transactions on Wireless Communications*, 2017, 16(8): 5218-5232.
- [57] Zhang, J., Zhou, Z., Li, S., Gan, L., Zhang, X., Qi, L., Xu, X. Dou, W. Hybrid computation offloading for smart home automation in mobile cloud computing, *Personal and Ubiquitous Computing*, 2018, 22(1): 121-134.
- [58] Wang, T., Wei, X., Tang, C., Fan, J. Efficient multi-tasks scheduling algorithm in mobile cloud computing with time constraints', *Peer-to-Peer Networking and Applications*, 2017, 11(4): 793-807.
- [59] Wang, Z., Zhao, Z., Min, G., Huang, X., Ni, Q., Wang, R. User mobility aware task assignment for mobile edge computing, *Future Generation Computer Systems*, 2018, 85: 1-8.
- [60] Zhang, J., Xia, W., Yan, F., Shen, L. Joint computation offloading and resource allocation optimization in heterogeneous networks with mobile edge computing, *IEEE Access*, 2018, 6: 19324-19337.
- [61] Elazhary, H. H., Sabbeh, S. F. The w5 framework for computation offloading in the internet of things, *IEEE Access*, 2018.
- [62] Chen, W., Wang, D. Li, K. Multi-user multi-task computation offloading in green mobile edge cloud computing, *IEEE Transactions on Services Computing*, 2018.
- [63] Wu, S., Mei, C., Jin, H. Wang, D. Android unikernel: Gearing mobile code offloading towards edge computing, *Future Generation Computer Systems*, 2018.
- [64] Liu, L. Chang, Z. Guo, X. Socially-aware dynamic computation offloading scheme for fog computing system with energy harvesting devices, *IEEE Internet of Things Journal*, 2018.
- [65] Rahbari, D., Nickray, M. Task offloading in mobile fog computing by classification and regression tree. *Peer-to-Peer Networking and Applications*, 2019, 1-19.
- [66] Tang, Z., Zhou, X., Zhang, F., Jia, W., Zhao, W. Migration modeling and learning algorithms for containers in fog computing, *IEEE Transactions on Services Computing*, 2018.
- [67] Mohan, N. Kangasharju, J. Placing it right! optimizing energy, processing, and transport in edge-fog clouds, *Annals of Telecommunications*, 2018: 1-12.
- [68] Lyu, X., Tian, H., Jiang, L., Vinel, A., Maharjan, S., Gjessing, S., Zhang, Y. Selective offloading in mobile edge computing for the green internet of things, *IEEE Network*, 2018, 32(1): 54-60.
- [69] Du, J., Zhao, L., Feng, J., Chu, X. Computation offloading and resource allocation in mixed fog/cloud computing systems with min-max fairness guarantee, *IEEE Transactions on Communications*, 2017.
- [70] Shuja, J., Gani, A., Ko, K., So, K., Mustafa, S., Madani, S.A. Khan, M.K. Sim-dom: A framework for simd instruction translation and offloading in heterogeneous mobile architectures, *Transactions on Emerging Telecommunications Technologies*, 2018, 29(4): e3174.



ARTICLE

Development of IoT Based Mobile Robot for Automated Guided Vehicle Application

M. A. S. M. Alhaddad¹ **K. Kamarudin^{1,2*}**

1. School of Mechatronic Engineering, University Malaysia Perlis, Pauh Putra Campus, 02600, Arau, Perlis, Malaysia

2. Center of Excellence for Advanced Sensor Technology, University Malaysia Perlis, Lot 16-21, Jalan Jejawi Permatang, 02600, Arau, Perlis, Malaysia

ARTICLE INFO

Article history

Received: 22 July 2019

Accepted: 28 October 2019

Published Online: 31 October 2019

Keywords:

Automated guided vehicle

Mobile robot

Internet of things

Mobile app

RFID

ABSTRACT

Mobile robot has been one of the researches focuses in this era due to the demands in automation. Many industry players have been using mobile robot in their industrial plant for the purpose of reducing manual labour as well as ensuring more efficient and systematic process. The mobile robot for industrial usage is typically called as Automated Guided Vehicle (AGV). The advances in the navigation technology allows the AGV to be used for many tasks such as for carrying load to pre-determined locations sent from mobile app, stock management and pallet handling. More recently, the concept of Industry 4.0 has been widely practiced in the industries, where important process data are exchange over the internet for an improved management. This paper will therefore discuss the development of Internet of Things (IoT) bases mobile robot for AGV application. In this project a mobile robot platform is designed and fabricated. The robot is controlled to navigate from one location to another using line following mechanism. Mobile App is designed to communicate with the robot through the Internet of Things (IoT). RFID tags are used to identify the locations predetermined by user. The results show that the prototype is able to follow line and go to any location that was preregistered from the App through the IoT. The mobile robot is also able to avoid collision and any obstacles that exist on its way to perform any task inside the workplace.

1. Introduction

The mobile robot is a robot that is capable of navigating around from one place to another in its environment without the need for physical or electro-mechanical guidance device. It has been used in many applications such as for remote sensing, transpor-

tation as well as to perform dangerous tasks like bomb defusing and minesweeper. Automated Guided Vehicle (AGV) is just the same as the mobile robot and it is a driverless car that can navigate to a predefined location by the user. Likewise, it is capable of following prescribed paths and it is usually used in the industries to transport raw materials to a preregistered location^[1]. The

**Corresponding Author:*

K. Kamarudin,

School of Mechatronic Engineering, University Malaysia Perlis, Pauh Putra Campus, 02600, Arau, Perlis, Malaysia; Center of Excellence for Advanced Sensor Technology, University Malaysia Perlis, Lot 16-21, Jalan Jejawi Permatang, 02600, Arau, Perlis, Malaysia;

Email: *kamarulzaman@unimap.edu.my

AGV application is important in the workplace to reduce the labourers in the industries, ease the physical strain on them and to improve the operational performance^[2].

In this project a mobile robot platform is designed using SOLIDWORKS for AGV application using the line following mechanism. The robot was controlled to navigate from one location to another through the Internet of Things (IoT) and RFID based tracking. The mobile robot should be able to avoid collision and any obstacles that could happen on its way to perform any task inside the workplace. The main idea of the robot's behaviour is to follow simple line algorithm and be able to perform the commands that will be sent from the mobile app. Therefore, this project involves designing, fabrication, integrating and interfacing robot's parts and sensors to IoT.

2. Related Works

IoT based automated guided vehicle deals with the material handling in the industry, which includes horizontal and vertical movements or combination of both. Material handling is an art of science which involves movement, packing, transporting. Material handling is an important activity in the production process. Out of total time spend on manufacturing 20% is for actual process & the remaining 80% is material handling moving the material from one location to another location. The above percentage should be altered according to the plant.

Yogesh Kakasaheb Shejwall and Sasi Kumar Gera^[2] developed an IoT system for an automated guided vehicle that deals with the demands in the manufacturing industry. The AGV will be able to follow a given path allocated for it. This will happen with the aid of Arduino, an ethernet shield and RFID^[3]. In this system, they can access and stored all the information in the device. this system will be sending the signals from the respective department using Bluetooth device and then the vehicle will receive these signals after that the vehicle will follow the path according to the given instruction. Delivering material to the respective location will be done after scanning the barcode of load material and after the vehicle accomplish that it will be back to the original position.

Nanda Kishor M and Prasad A P (2017)^[4]. An IoT Based smart car parking using line following robot. This system proposed a vehicle used in a smart city that when it enters the parking slot a series of led will glow indicating the dedicated parking slot and then the car will follow the led pattern using the concept of the line follower robot. The vehicle will be controlled by the Arduino which is the main controller of the vehicle and this vehicle will consist of an IR sensor, RF module, LED stripes,

line following robot. This system also constructs each car park as an IoT network, and the data that include the vehicle slot location and number of free slots in car park areas will be transferred to the data centre.

3. Methods

In this project Arduino will be the main controller to smoothly navigate the mobile robot. In this project there will be many procedures from designing the Three Dimensions (3D) model of the mobile robot using SOLIDWORKS, fabricating the designed parts, integrate the design parts and sensors to the mobile robot, implementation of the line following algorithm, development of IoT, interfacing IoT with the mobile App, interfacing the mobile app with the mobile robot through IoT and lastly testing the reliability of the line following mechanism in the mimicked industrial setup.

3.1 3D Design Progress

The mobile robot is designed (refer to Figure 4.1) in Computer Aided Design (CAD) programming 3D model using SOLIDWORKS where the robot will consist of two plates. Each plate got its own holes for wires to connect between the parts the lower plate will be attached with sensors, actuators and the Arduino. Nevertheless, the upper plate will be for the materials that will be transported from a place to another. There will be also six standoffs to hold and connect between the two plates. Two wheels will be in the front of the robot and a castor wheel will be in the back middle of the robot. two DC motors were also used to control the wheels. Also, there are the motor brackets to hold the DC motor and lastly there are the coupling to hold the DC motor with the wheel.

3.2 Line Following Mechanism

For accurate and smooth navigation for the mobile robot we have used a line following sensor contains of five IR sensor which are ML sensors, L sensor, middle sensor, R sensor and MR sensor to have smooth navigation through all the junctions in the way^[5]. There will be multiple junctions such as + junction, T junction and a wavy line. Hence, there will be many situations for the line following sensor. First situation is the ideal situation when the middle sensor is in the black line or the left sensor, middle sensor and right sensor is on the black line the mobile robot will move straight. Second situation is diagonally left when the right sensor or right sensor and most right sensor in on the black line the

mobile robot will move diagonally to the left by slowing the RPM of the right DC motor until the ideal situation occur to continue moving straight. Third situation is diagonally right when the lift sensor is on the black line or the left sensor with the most lift sensor is on the black line. Consequently, in this case the mobile robot will turn diagonally to the right by slowing the RPM^[6] of the left DC motor until the ideal situation occur to continue moving straight. Fourth situation is the situation where the Radio-frequency identification (RFID) will be used to control the right and left turn. If the RFID reader reads the RFID tag the mobile robot will turn left for one specific RFID tag by stopping the right DC motor. And will turn right for another specific RFID tag by stopping the lift DC motor.

3.3 Radio-Frequency Identification (RFID)

Radio-frequency identification uses electromagnetic fields to automatically identify and track tags attached to objects. To make our mobile robot smoother and to avoid any error that could happen we have used the RFID sensors to have a smoothly left and right turn. This will be working as there will be RFID reader stick on the bottom of the mobile robot and also there will be RFID cards on the floor near to the line that the robot will follow whenever the RFID reader reads the RFID tag it will perform a specific task such as turn right or turn left. RFID tag also used to define multiple locations which we will have four locations each location will have a specific RFID tag whenever the reader reads the RFID tag of the location that the user entered through the mobile APP the mobile robot will stop for a short time until the load has unloaded from the mobile robot after that the mobile robot will go back to the initial position.

3.4 Collision Avoidance

In order to avoid a collision that could obstruct the mobile robot on his way, an Ultrasonic sensor has been used. Ultrasonic sensor measures if there is any obstacle in front of the mobile robot and there will be two options to decide if the obstacle is far from the mobile robot then it will slow the mobile robot if its near it will stop the mobile robot from moving forward. By implementing this we will be able to make our mobile robot able to avoid any obstacles that may happen in the way of the mobile robot to its destination.

3.5 IoT Implementation to The Mobile App

To control our mobile robot remotely IoT will be used to

interface a mobile App with the mobile robot. An open platform has been chosen to control the data from the App to the mobile robot we have choose Thingspeak as an IoT platform. The app will be designed through the MIT App inventor which is able to interface with hardware projects through internet^[7]. this App will contain five buttons each button defines a specific location in the workspace and one button will be used to stop the mobile robot as there will be up to four locations. The app will also be able to show where the mobile robot is actually at. And it will send us a notification to update us whether the robot is already reaching the desired location or not. Moreover, there will be a label to communicate with the Thingspeak to show a notification from the Thingspeak platform whether the commands have been sent successfully or not. Therefore, if the commands sent to the Thingspeak from the App successfully it will give a notification stating that the command has been sent successfully. Nevertheless, if there was any error with the communication between the Thingspeak and the app we will receive a notification stating that there was an error with trying sending commands. There is another label will be used to show if the App is connected to the internet or not if it's connected it will show that its connected if it's not it will also show it's not connected in a label message somewhere inside the App.

4. Results and Discussion

This section discusses the results including the 3D design, fabrication of the parts, line following mechanism and interfacing the mobile robot with mobile App.

4.1 3D Design

The 3D design of the robot was successfully done and completed using the CAD programming software which is SOLIDWORKS as shown in Figure 4.1. The design is suitable for the mobile robot in the project and it consists of a double deck or two plates 300 mm length, 250 mm width and 10mm for the thickness of each plate, stand-offs also were designed in 130mm as a length to hold and connect between the plates. Furthermore, two wheels were also designed to navigate the mobile robot from location to another. However, the designing also includes the roller-coaster, DC motor, a bracket to hold and support the DC motor to keep it stationary and a coupling to connect between the DC motor and the wheel. Figure 4.1 Shows the 3D design of the mobile robot. In addition, the mobile robot has been fabricated and print out into A 3D model as shown in Figure 4.2.



Figure 4.1. Designed Mobile robot

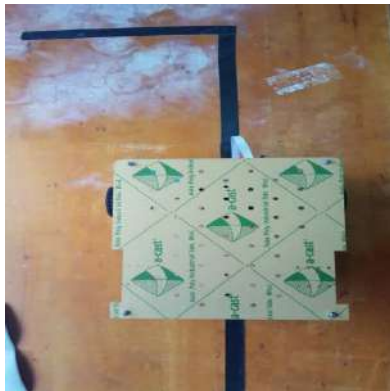



Figure 4.2. Fabricated mobile robot

4.2 Line Following Mechanism

Arduino UNO is used as the main controller to control the mobile robot in the workspace. The mobile robot is able to follow the line smoothly and pass all the junctions which are the + junction, T junction and wavy way using the line follower that contains of five IR sensors which are most right sensor, right sensor, middle sensor, right sensor, most right sensor. The line follower sensor will sense the black line in the floor if the middle sensor senses the black line the mobile robot will go forward by setting the DC motor's RPM to the same value. Nonetheless, if the left sensor senses the black line the mobile robot will move right by stopping the left motor and moving the right DC motor. For example, left DC motor RPM equals to the zero and right DC motor equals to two hundred by applying this the mobile robot will move right. Conversely, if the right sensor senses the black line the mobile robot will move left by stopping the right DC motor and moving the left DC motor. For example, we set the right DC motor equals to zero and the right DC motor equals to two hundred by applying this the robot will go left. There are other situations where two of the IR sensors are in the black line either the left sensor and the most left sensor with the

middle sensor or the right sensor with the middle sensor are on the black line. In this situation the mobile robot will not be in the middle of the black line so this problem needs to be solved by playing with the RPM of the DC motors. For example, if the black line is not in the middle of the line we will turn diagonally the mobile robot either to the left or to the right by increasing the RPM of one DC motor and decreasing the RPM of the other DC motor by applying this the mobile robot will turn until it meets the ideal situation which is when the mobile robot is in the middle of the black line. In other words, until the middle IR sensor of the line follower sensor sense the black line. For the locations we have decided to use the RFID to control the decision either to turn completely right or left this has been done whenever the RFID reader reads the RFID card tag. The RFID card tags are located next to the line so whenever the RFID reader reads the RFID card tag it will decide which way will take based on the code. In our code location A, the mobile robot will follow the line until the RFID reads a specific RFID card tag and then it will turn right to location A once it reaches location A it will stop for ten seconds to unload the load then it will rotate and go back to the initial position. For location B the mobile robot will follow the line until the RFID reader reads the RFID card tag for location B then it will turn left ahead to location B once it reach location B the mobile robot will rotate and go back to the initial position and the same procedure for the other locations which are C and D. The mobile robot will keep going to any desired locations entered by the user through the app. Furthermore, it will stop if there is any obstacle in front of the mobile robot this has been done using ultrasonic sensor if the distance between the obstacle and the mobile robot is far the mobile robot will slowdown its speed by decreasing the DC motors RPM. Nevertheless, if the obstacle is near to the mobile robot the mobile robot will stop moving until this obstacle get removed. In Table 4.1 shows the result of the four trajectories of the line following mechanism

Table 4.1 Results of The Line Following Mechanism

No.	Trajectory	No. of trails succeed	Percentage	Figure
1.	L shape	10 out of 10	100%	

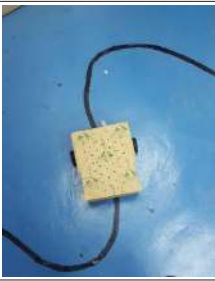


2.	S shape	9 out of 10	90%	
3.	Straight line	10 out of 10	100%	
4.	O shape	8 out of 10	80%	

Table 4.1 shows the result of the line following in four trajectories of an experiment of ten trails for each trajectory which are L, O, straight line and S shape. However, straight line and L shape got a 100 % accuracy. And S shape got 90% accuracy. Nevertheless, O shape got 80% accuracy. The mobile robot will be placed in initial position and if the mobile robot moves and came back to the initial position it will be success and miss of the line it will be fail even though if the mobile robot came back to catch up with the line.

4.3 Interfacing Mobile Robot with Mobile App

In order to navigate the mobile robot and smoothly let it follow the line to go to the desired locations. An IoT platform has been established which is the ThingSpeak to act as a data server in interfacing the mobile robot with the app. ThingSpeak will be receiving the data from the app and it will send it to the Arduino which is the main controller of the mobile robot. The mobile app has been also designed using MIT App inventor which will be sending commands to the mobile robot through the ThingSpeak. In the MIT app. Thus, there is five buttons first button define location A whenever this button pressed this button it will send a value of one to the ThingSpeak and then the Arduino will receive this coming value which is defines

location A. However, the second button define location B once this button pressed it will send a value of two to the ThingSpeak and the Arduino will retrieve this coming data which defines location B. Moreover, the third button define location C once this button pressed a value of three will be sent to the ThingSpeak and Arduino will receive this data which defines location C. Nonetheless, the fourth button define location D once the fourth button pressed a value of four will be sent to the ThingSpeak and then the Arduino will receive this data which defines location D. Furthermore, the fifth button has been created to stop the mobile robot from moving once we press this button a value of zero will be sent to the ThingSpeak then the Arduino will receive this data which is defined to stop the mobile robot from moving whenever this button pressed. However, this app will also show us where the current location of the mobile robot is actually this location will be defined using the RFID. There will also be a label to show us the success of sending the commands if the commands have been sent successfully it will show us that the command has been sent successfully is not it will show that there is an error with trying sending command. Another label has been created to show the status of the internet connection whether the app is connected to the internet or not if it is connected it will show that is connected if it is not connected it will show that it is not connected. Figure 4.4 Shows the features of the App. However, In Table 4.2 shows the results of the AGV interfaced with IoT.

Table 4.2 Results of the IoT Interfaced with the AGV

No.	LOCATION	Success of the move	Time travel per seconds
2.	LOCATION B	Success	4.6
3.	LOCATION C	Success	4.8
4.	LOCATION D	Fail	Fail
5.	LOCATION A	Success	5
6.	LOCATION B	Fail	Fail
7.	LOCATION C	Success	4.9
8.	LOCATION D	Success	4.8
9.	LOCATION A	Fail	Fail
10.	LOCATION B	Success	4.7

Table 4.2 shows the result of an experiment to send the mobile robot from the initial position to a predetermined location using the mobile App to send commands. However, ten commands have been sent from the mobile app as shown in Figure 4.4 to the mobile robot through IoT to navigate the mobile robot. Out of ten commands there are seven commands has been sent successfully and the mobile robot has gone to the desired location from its initial position and be back to its initial position in an average

time of 4.83 seconds. Furthermore, three out of the ten commands the command has not been sent successfully. Nevertheless, Figure 4.3 shows the Setup of AGV in order to navigate the mobile robot from one location to another. It shows the black line and the RFID cards along the black line.

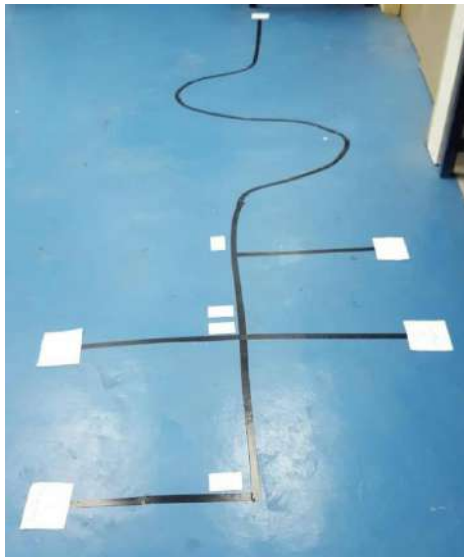


Figure 4.3 Setup for the mobile robot

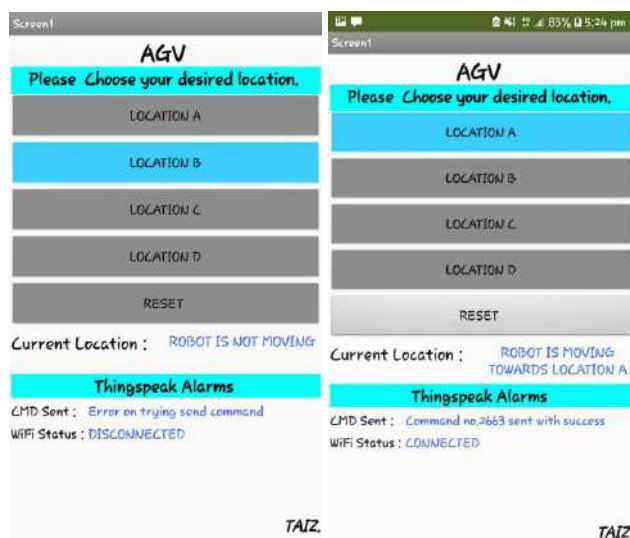


Figure 4.4 Mobile APP layout and Design

5. Conclusion

A mobile robot platform was designed and fabricated to replicate an AGV system. The robot was controlled to navigate from one location to another using line following mechanism with Internet of Things (IoT) based communication. RFID tags were used to identify the preregistered locations along the path. The results show that the robot was able to follow line and arrived at any location that was instructed from the Mobile App through the IoT communication. The mobile robot was also able to avoid collision and any obstacles that exist on its way during the operation. To improve the system, a laser scanner or Kinect camera can be added on top of the mobile robot to perform feature or facial recognition. This recommendation can help improve the obstacle avoidance and therefore provide a more reliable operation for AGV application.

References

- [1] L. Tang and S. Yuta. Indoor navigation for mobile robots using memorized omni-directional images and robot's motion. *Proc. IEEE/RSJ Int. Conf. Intell. Robot. Syst.*, no., 2002: 269–274.
- [2] Y. K. Shejwal and S. K. Gera. Iot based automated guide vehicle. 2018: 3256–3259.
- [3] R. Turbulence and D. N. Simulation. Introduction 1.1. no. Ddc, 1845: 1–12.
- [4] I. Journal, O. Electrical, and D. Communication. Iot based smart car parking using line following robot 1, 2017.
- [5] N. Hayat, D. Khushi, and M. Rashid. Algorithm for Line Follower Robots to Follow Critical Paths with Minimum Number of Sensors. *Int. J. Comput.*, 2017, 24(1): 13–22.
- [6] M. Z. Baharuddin, I. Z. Abidin, and S. S. K. Mohideen. Analysis of Line Sensor Configuration for the Advanced Line Follower Robot. *Proc. Student Conf. Res. Dev. (SCOREd)*, Bangi, Selangor, Malaysia., 2006: 1–12.
- [7] N. Lao. CloudDB: Components for exploring shared data with MIT app inventor. *Proc. - 2017 IEEE Blocks Beyond Work. B B*, 2017, 2017: 109–110.

Author Guidelines

This document provides some guidelines to authors for submission in order to work towards a seamless submission process. While complete adherence to the following guidelines is not enforced, authors should note that following through with the guidelines will be helpful in expediting the copyediting and proofreading processes, and allow for improved readability during the review process.

I . Format

- Program: Microsoft Word (preferred)
- Font: Times New Roman
- Size: 12
- Style: Normal
- Paragraph: Justified
- Required Documents

II . Cover Letter

All articles should include a cover letter as a separate document.

The cover letter should include:

- Names and affiliation of author(s)

The corresponding author should be identified.

Eg. Department, University, Province/City/State, Postal Code, Country

- A brief description of the novelty and importance of the findings detailed in the paper

Declaration

v Conflict of Interest

Examples of conflicts of interest include (but are not limited to):

- Research grants
- Honoria
- Employment or consultation
- Project sponsors
- Author's position on advisory boards or board of directors/management relationships
- Multiple affiliation
- Other financial relationships/support
- Informed Consent

This section confirms that written consent was obtained from all participants prior to the study.

- Ethical Approval

Eg. The paper received the ethical approval of XXX Ethics Committee.

- Trial Registration

Eg. Name of Trial Registry: Trial Registration Number

- Contributorship

The role(s) that each author undertook should be reflected in this section. This section affirms that each credited author has had a significant contribution to the article.

1. Main Manuscript

2. Reference List

3. Supplementary Data/Information

Supplementary figures, small tables, text etc.

As supplementary data/information is not copyedited/proofread, kindly ensure that the section is free from errors, and is presented clearly.

III . Abstract

A general introduction to the research topic of the paper should be provided, along with a brief summary of its main results and implications. Kindly ensure the abstract is self-contained and remains readable to a wider audience. The abstract should also be kept to a maximum of 200 words.

Authors should also include 5-8 keywords after the abstract, separated by a semi-colon, avoiding the words already used in the title of the article.

Abstract and keywords should be reflected as font size 14.

IV . Title

The title should not exceed 50 words. Authors are encouraged to keep their titles succinct and relevant.

Titles should be reflected as font size 26, and in bold type.

IV . Section Headings

Section headings, sub-headings, and sub-subheadings should be differentiated by font size.

Section Headings: Font size 22, bold type

Sub-Headings: Font size 16, bold type

Sub-Subheadings: Font size 14, bold type

Main Manuscript Outline

V . Introduction

The introduction should highlight the significance of the research conducted, in particular, in relation to current state of research in the field. A clear research objective should be conveyed within a single sentence.

VI . Methodology/Methods

In this section, the methods used to obtain the results in the paper should be clearly elucidated. This allows readers to be able to replicate the study in the future. Authors should ensure that any references made to other research or experiments should be clearly cited.

VII . Results

In this section, the results of experiments conducted should be detailed. The results should not be discussed at length in

this section. Alternatively, Results and Discussion can also be combined to a single section.

VIII. Discussion

In this section, the results of the experiments conducted can be discussed in detail. Authors should discuss the direct and indirect implications of their findings, and also discuss if the results obtain reflect the current state of research in the field. Applications for the research should be discussed in this section. Suggestions for future research can also be discussed in this section.

IX. Conclusion

This section offers closure for the paper. An effective conclusion will need to sum up the principal findings of the papers, and its implications for further research.

X. References

References should be included as a separate page from the main manuscript. For parts of the manuscript that have referenced a particular source, a superscript (ie. [x]) should be included next to the referenced text.

[x] refers to the allocated number of the source under the Reference List (eg. [1], [2], [3])

In the References section, the corresponding source should be referenced as:

[x] Author(s). Article Title [Publication Type]. Journal Name, Vol. No., Issue No.: Page numbers. (DOI number)

XI. Glossary of Publication Type

J = Journal/Magazine

M = Monograph/Book

C = (Article) Collection

D = Dissertation/Thesis

P = Patent

S = Standards

N = Newspapers

R = Reports

Kindly note that the order of appearance of the referenced source should follow its order of appearance in the main manuscript.

Graphs, Figures, Tables, and Equations

Graphs, figures and tables should be labelled closely below it and aligned to the center. Each data presentation type should be labelled as Graph, Figure, or Table, and its sequence should be in running order, separate from each other.

Equations should be aligned to the left, and numbered with in running order with its number in parenthesis (aligned right).

XII. Others

Conflicts of interest, acknowledgements, and publication ethics should also be declared in the final version of the manuscript. Instructions have been provided as its counterpart under Cover Letter.

Journal of Electronic & Information Systems

Aims and Scope

Journal of Electronic & Information Systems publishes original research papers that offers professional review and publication to freely disseminate research findings in areas of Networks and Telecommunication, Human–Computer Interaction, Data Management, High Voltage Engineering and more. The Journal focuses on innovations of research methods at all stages and is committed to providing theoretical and practical experience for all those who are involved in these fields.

Journal of Electronic & Information Systems aims to discover innovative methods, theories and studies in its field by publishing original articles, case studies and comprehensive reviews.

The scope of the papers in this journal includes, but is not limited to:

- Networks and Telecommunication
- Human–Computer Interaction
- Data Management
- High Voltage Engineering
- E-Learning Technologies
- E-Commerce Technology
- Computation
- Power Electronics
- Digital Control Systems
- Electronic Ignition Systems
- Digital Communication systems
- Analytics, Business Intelligence and Decision Support Systems

Bilingual Publishing Co. (BPC)

Tel: +65 65881289

E-mail: contact@bilpublishing.com

Website: www.bilpublishing.com

About the Publisher

Bilingual Publishing Co. (BPC) is an international publisher of online, open access and scholarly peer-reviewed journals covering a wide range of academic disciplines including science, technology, medicine, engineering, education and social science. Reflecting the latest research from a broad sweep of subjects, our content is accessible world-wide—both in print and online.

BPC aims to provide an analytics as well as platform for information exchange and discussion that help organizations and professionals in advancing society for the betterment of mankind. BPC hopes to be indexed by well-known databases in order to expand its reach to the science community, and eventually grow to be a reputable publisher recognized by scholars and researchers around the world.

BPC adopts the Open Journal Systems, see on ojs.bilpublishing.com

Database Inclusion



Asia & Pacific Science
Citation Index



Creative Commons



China National Knowledge
Infrastructure



Google Scholar



Crossref



MyScienceWork

Bilingual Publishing Co. is a company registered in Singapore in 1984, whose office is at 12 Eu Tong Sen Street, #08-169, Singapore 059819, enjoying a high reputation in Southeast Asian countries, even around the world.



**BILINGUAL
PUBLISHING CO.**
Pioneer of Global Academics Since 1984

Tel: +65 65881289

E-mail: contact@blipublishing.com

Website: www.Blipublishing.com

ISSN 2661-3204



9 772661 320193